Additive Manufacturing 38 (2021) 101752

Contents lists available at ScienceDirect

Additive Manufacturing

journal homepage: www.elsevier.com/locate/addma

Research Paper

Design of particle dampers for additive manufacturing

Tobias Ehlers [a,*], Sebastian Tatzko [b], Jörg Wallaschek [b], Roland Lachmayer [a]

[a] Institute of Product Development (IPeG), Gottfried Wilhelm Leibniz Universität Hannover, An der Universität 1, 30823 Garbsen, Germany
[b] Institute of Dynamics and Vibration Research (IDS), Gottfried Wilhelm Leibniz Universität Hannover, An der Universität 1, 30823 Garbsen, Germany

ARTICLE INFO

Keywords:
Laser powder bed fusion (LPBF)
Particle damping
Additive manufacturing (AM)
Functional integration
Design for additive manufacturing (DfAM)

ABSTRACT

Damping mechanisms are a crucial factor for influencing the vibration behavior of dynamic systems. In many applications vibrations are undesirable and need to be reduced by appropriate measures. For instance, vibrations in vehicles can reduce driving comfort or in civil engineering resonance damage can occur in constructions. An interesting and cost-effective way of increasing damping is particle damping. In modern processes of additive manufacturing, like laser powder bed fusion (LPBF), unmelted powder can be left inside a structure on purpose after making and thus producing integrated particle dampers already. Additively manufactured particle damping has not yet reached the industrial level because there are no detailed specifications for the design process. This includes the modeling of (non-linear) dynamic properties, based on numerous design parameters. The state of the art reveals that the effect of particle damping has been convincingly demonstrated, but transferability of the obtained information is still limited. In this paper the effect of particle damping is investigated experimentally with LPBF manufactured beam structures made of AlSi10Mg. Particle damping is evaluated in terms of performance curves for different beam parameter sets. The aim is to help the designer, who needs to keep amplitudes in certain range to estimate the damping of the potential particle damper via the given performance curves. Damping is determined via experimental modal analysis by impulse excitation. The response is evaluated in the frequency domain using the Circle-Fit method with a focus on the beams first bending mode of vibration. Beyond that, a significantly increased damping could be verified up to the seventh bending mode covering a frequency range between 600 Hz and 18k Hz. Damping through particle-filled cavities shows up to 20 times higher damping compared to the same component with fused powder.

1. Introduction

By introducing particles, the structural damping can be significantly increased by a factor of more than 20 with considerably reduced sound radiation [1–9]. In addition, vibrations can be reduced broadband from a few Hz to several kHz [10–13]. One way of efficiently integrating particle damping into components is additive manufacturing, in particular laser powder bed fusion (LPBF) [2–9,14–16]. In keeping with the “Complexity for free” [17] principle, “Damping for free” applies to additively manufactured components, since neither mass nor costs increase with increasing damping compared to the additively manufactured reference component.

Due to the high degree of design freedom, LPBF is particularly suitable for the production of complex structural components [18–22]. The material can be located at the highly stressed areas so that load-adapted lightweight structures with excellent mechanical properties are possible [23]. However, lightweight structures, especially aerodynamically optimized integral components, are often susceptible to vibrations [24]. Powder bed-based processes are particularly suitable for the construction of integrated particle dampers to counteract this susceptibility [2–9,14]. In the additive manufacturing process, the powder is left unfused in cavities provided inside the structure, which further increases the functional integration of the manufactured component by the effect of particle damping. In addition, particle dampers are manufactured additively if other damping mechanisms cannot be installed due to lack of space or mass restrictions or if natural vibration forms have to be specifically adapted locally. Additive manufacturing is also used if the cavity for particle damping cannot be manufactured in any other way.

Particle dampers in general have long been used in a variety of applications [1]. In contrast, the use of additively manufactured particle damping has only recently gained attention, cf. [25], but has not yet reached the industrial level. This can be attributed to the fact that there

* Corresponding author.
E-mail addresses: ehlers@ipeg.uni-hannover.de (T. Ehlers), tatzko@ids.uni-hannover.de (S. Tatzko), wallaschek@ids.uni-hannover.de (J. Wallaschek), lachmayer@ipeg.uni-hannover.de (R. Lachmayer).

https://doi.org/10.1016/j.addma.2020.101752
Received 17 July 2020; Received in revised form 29 October 2020; Accepted 3 December 2020
Available online 13 December 2020

are no detailed specifications for the design of additively manufactured particle dampers. This includes the modeling of (non-linear) dynamic properties, based on numerous design parameters and information on the service life. So far, only isolated components such as cutting tool holders or braking disks have been investigated along with selected fundamental studies [2–9,14]. The results have in common that the effect of particle damping has been convincingly demonstrated, but transferability of the obtained information is still limited.

Relevant design data for choosing a vibration reduction measure are excitation force, frequency and vibration amplitude [26]. This paper examines the nonlinear effects of particle damping in terms of performance curves. To this end, force- and frequency-dependent damping curves are determined from measurements on laser melted AlSi10Mg beams. A Design of Experiment (DoE) is the starting point in the methods section of the paper including error estimation and reproducibility of the measurement results. Moreover, the beam and cavity geometries are defined in the DoE. With an impulse hammer excitation, the effect of particle damping is evaluated in the range of 600–18,000 Hz, the focus being mainly on the evaluation of the first bending mode. The effect of particle damping is evaluated in each case with respect to the fully fused (solid) beams. The aim is to obtain a comprehensive amount of data in order to be able to transfer the damping effect to other components. Based on modal data, the dynamic response of beams may be transferred to similar structures by interpolation of the presented results. The results could also serve as a basis for establishing references for the expected damping of certain cavities.

2. Review

Additive manufacturing is already used to systematically influence the vibration behavior of components [27–29]. For example, lattice structures can be integrated into laser melted structures to shift natural frequencies into uncritical frequency ranges, increase damping or save mass. The latter effect is of particular interest in lightweight construction.

A further increase in damping is possible if powder is placed in cavities, with or without lattice structures, exploiting the particle damping effect [8,14]. Particles are either embedded in cavities of a structure, or the particle damper is mounted as an independent system on the vibrating structure [1]. Through the combined forces of inelastic impacts and friction, either particle/particle or particle/wall interaction, kinetic energy is absorbed from the vibrating main structure resulting in increased damping [1,12]. A simplified diagram of a particle damper is shown in Fig. 1. Due to the numerous advantages described below, conventionally manufactured particle dampers are very common.

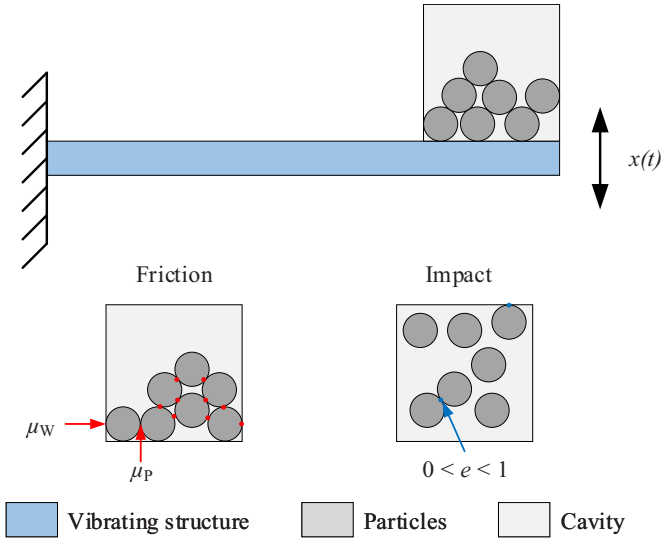

Fig. 1. Schematic diagram of a particle damper.

Simple and low-cost design: Depending on the design, particle dampers usually have several, usually spherical particles or balls [1,30]. These are either put into a container which is fixed to the structure or into cavities of the structure [1], which has only a limited effect on structural mass and stiffness [1,2,31]. Particle dampers are naturally a passive system, therefore no energy is required [1,12]. Overall, it is a cost-effective method for reducing vibrations [1,32–34].

High operating life: Particle dampers can be permanently used in harsh environmental conditions such as severe cold e.g. in cryogenic applications [35] or in oiled environments [1,31]. They show little wear and are low maintenance allowing them to be used where other types of dampers would fail [1]. Furthermore, particle dampers can extend the lifespan of dynamically loaded components, due to reduced stresses [32].

Temperature resistant: Particle dampers can be used at temperatures up to 2000 °C using appropriate particles [1,36]. This requires the operating temperature to be lower than the melting temperature of the particles. For example, tungsten powder can be used for high temperature applications [1]. Particle dampers can therefore be used in temperature ranges where other damping mechanisms would fail [37].

Broadband damping: Particle dampers are suitable for both low-frequency, few Hz and high-frequency applications up to several kHz [10–13].

2.1. Design parameter

Energy dissipation in particle dampers is caused by a combination of different loss mechanisms, which are generally nonlinear and are influenced by various system parameters such as cavity length, cavity width, cavity height, natural frequency and excitation force [34,37]. Design parameters for damping have already been investigated for conventionally manufactured particle dampers [10,11,30,31,33–38]. Though the influence of certain parameters on the damping performance may be estimated, there is currently no reliable modeling of the relationships.

2.1.1. Excitation level

With many small particles, the frictional forces between particles must first be overcome before they can move in the damper [10]. Only when particle motion and particle interactions occur, the damping increases [10] and initially rises further as the amplitude increases [33].

Fowler et al. also confirm that the maximum system damping depends on the excitation level. If the excitation level is higher or lower than the optimum, the system damping decreases. This relationship is closely connected to cavity dimensions, especially the size of the cavity in the direction of the oscillating motion [37].

2.1.2. Particle mass

The primary factor for energy dissipation is the particle mass and the excitation amplitude [39]. Some studies recommend to use tungsten as particle material due to its high density [11]. Particle mass must be considered in terms of its coupling to other parameters [30]. In experiments with increasing mass, the packing density and the particle number also increase. Research by Hollkamp and Gordon showed that with increasing mass the system damping increases up to a certain value and then remains constant. At maximum filling of the cavity the system damping drops significantly, which is due to high packing forces on particle zones that prevent them from moving [10,30]. Fowler et al. added that with increasing mass there is also a significant shift in the natural frequency [37]. However, even with a relatively small mass ratio, particle dampers can considerably reduce the vibrations of structures with low damping [10].

2.1.3. Packing density

The packing density indicates the ratio of the volume of all particles in relation to the cavity volume. It is difficult to investigate the packing density separately because the total particle mass is directly coupled. Hollkamp and Gordon bypassed this problem by mixing different materials with different densities to vary the packing density. As a result, an optimal packing density of 45% was identified. In the range from 67% to 78% the system damping decreases only slightly, at 100% packing density no system damping is apparent [30]. The reason for an optimum is that at a low packing density the number of particles and thus the number of friction and impact contacts is low, whereas at a packing density of 100% the movement of the particles is reduced. In other studies, a similar packing density of 40–80% was specified in order to achieve well balanced friction and collision forces for high energy dissipation [16,40,41].

2.1.4. Dimensions/cavities

In the gravitational direction, large cavity dimensions and high filling ratios can restrict the movement of lower particle layers [10,30]. This effect limits the maximum effective size of the cavity in the direction of gravity. The optimum cavity height needs to be determined individually for each application [30]. On the other hand, the system damping is low with small cavities [10]. Basically, the particle damper should be installed where the expected deflection of the main structure is highest or where the highest kinetic energy is present [30]. Furthermore, other parameters such as particle size/diameter, particle shape, particle material, particle hardness, etc. play a role in the effect of particle damping [10,11,16,30,31,38,42].

2.2. Production of laser fused particle dampers

Powder-bed based processes allow the component and the integrated particle damper to be manufactured in one production step [2–9,14–16]. LPBF in particular opens up the potential to leave unmelted powder in cavities and thus increase component damping [2–9,14–16]. The integration of the particle damper also saves production time, as the area in which the unfused particles are to be located does not have to be melted [16]. Accordingly, the integration of particle damping does not counteract the high degree of functional integration and economic efficiency of additive manufacturing [8,16,43].

Fig. 2 shows the manufacturing process of particle damped gears in the LPBF. Due to the layering principle of LPBF systems, it is not easily possible to vary the packing density of the powder in the cavities, which is approx. 50–60% [44] and thus lies within the range to achieve high damping [30]. Several particles can be fused to a larger one or finer/-coarser powder can be used to vary the packing density in the LPBF [16]. A limitation of the production process is that the powder exhibits the same chemical composition as the component. This problem can be overcome by integrating a multi-material coater into the laser powder bed fusion process [45,46].

Fig. 3 describes the manufacturing restrictions for particle filled cavities. These manufacturing restrictions apply to all LPBF systems and materials, but the values given differ. When designing the cavities, it should be taken into account that lattice support structures must be used beyond a certain down-skin angle. Integrated lattice structures are to be used, since separate supporting structures cannot be removed later [21,48]. Alternatively, self-supporting structures can be designed [23]. It must be taken into account that the surfaces in the cavities cannot be subsequently machined [49]. For example, the surface roughness of dynamically loaded components could be a reason for crack initiation [49]. The minimum dimensions for holes or gaps are determined by the fact that the powder can only move freely to a limited extent in narrow cavities [48,50]. It follows that the powder can act like a solid mass during component vibrations and no longer contributes to increasing component damping. When determining the minimum wall thickness, it must be noted that the wall thickness is reduced by abrasive wear due to particle/wall interaction [6].

2.3. Applications and research activities

Künneke and Zimmer investigate the effects of particle damping on an anchor plate for an electromagnetic spring-applied brake [8,9]. During braking, the electromagnet is switched off and the anchor plate impulses the rotor followed by vibrations which lead to an undesired noise emission. For a brake disc made of AISI 316L stainless steel with powder damping manufactured by LPBF, sound pressure measurements showed an average reduced sound emission of 7.86 db(C) [8].

Künneke and Zimmer also examine laser melted samples of AISI 316L stainless steel with powder filling in free decay. They find that as the cavity volume increases, damping increases, while the decay time is reduced by up to 83%. In addition, Künneke and Zimmer note that a cavity partitioning leads to a reduction of damping for equivalent cavity volumes [8].

In the work of Vogel et al. and Biermann et al., laser melted cutting tool holders made of 1.2709 stainless steel, with powder embedded in them, are examined [14,15]. Due to the powder embedding, a reduced vibration amplitude and a shift in the natural frequency can improve the operating conditions, the dynamic behavior and the tool life [14,15].

Scott-Emuakpor et al. investigate forced vibrations of particle-damped beams made of Inconel 718 [2–7] and AISI 316L stainless steel [7]. The beams are clamped to a shaker and their vibrations are measured with a laser vibrometer while the shaker vibrations are tracked additionally with an accelerometer. Damping is calculated by means of the second and third bending mode vibration, since the first mode is affected too much by the clamping. Using up to 4% of the beams volume as cavity size, the component damping can be increased by a

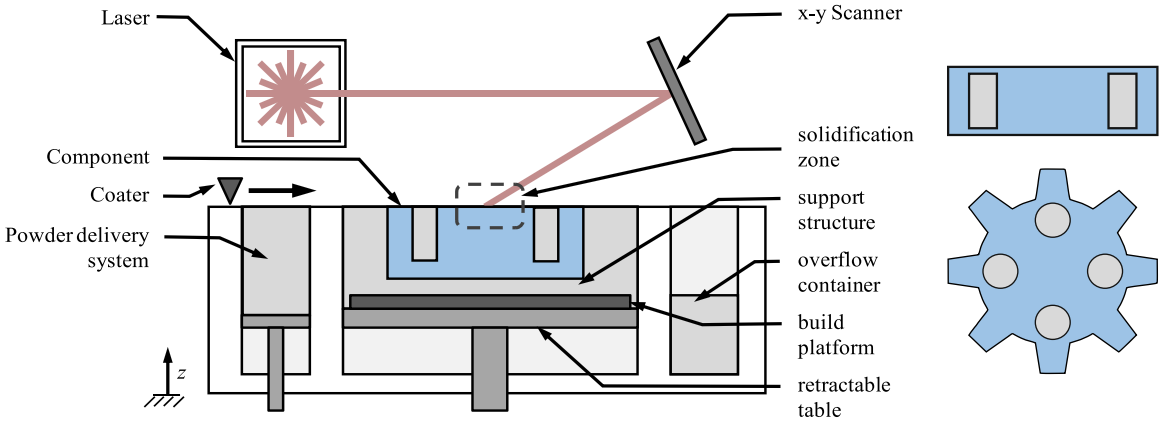

Fig. 2. Laser powder bed fusion of a particle damped gear according to [43,47].

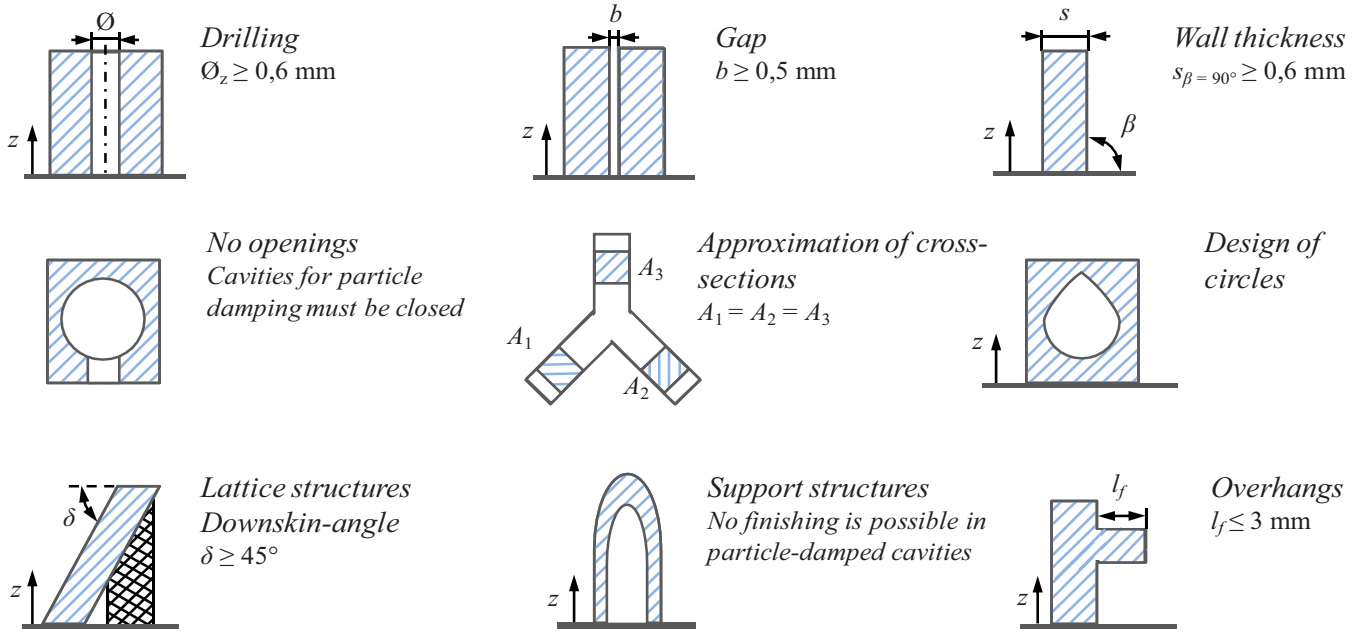

Fig. 3. Manufacturing restrictions for laser powder bed fusion of particle-filled cavities, the specified values apply to AlSi10Mg manufactured on EOS M280 according to [43,47,51].

factor of up to sixteen [2,6]. Furthermore, a damping model could be constructed with the help of a regression analysis from the results [4,5,7].

2.4. Experimental characterization of damping

Determining structural damping of a component experimentally can be done, either in the time domain or in the frequency domain. A common frequency domain method is called circle-fit [52,53]. The frequency response function (FRF) is reconstructed as Nyquist curve in the complex plane, where each resonance is forming a circle. Both eigenfrequency ω and damping ratio D can be calculated using the circle-fit method according to Eqs. (1) and (2), respectively [52].

$$\omega = \frac{\Omega_b - \Omega_a}{\varphi_b - \varphi_a} \times (\pi - \varphi_a) + \Omega_a \tag{1}$$

$$D = \frac{{\Omega_b}^2 - {\Omega_a}^2}{2 \times \omega \times (\Omega_a \times \tan(\Theta_a) - \Omega_b \times \tan(\Theta_b))} \tag{2}$$

Here Ω represents the natural angular frequency and φ and Θ the corresponding angles. The indices a and b represent measured points. Fig. 4 shows exemplarily an FRF section with one resonance peak and a corresponding circle-fit approximation.

Damping can be estimated for different value pairs Ω_a and Ω_b which can be averaged to increase robustness of the procedure.

Considering both conventional and additively manufactured particle dampers there is no generally valid mathematical description of damping performance available. Although parameter influences can be estimated more transferable data on frequency and amplitude dependency is needed to support engineers in the damper design phase. As complicated dynamic systems may be approximated by equivalent substitute systems, it is useful to determine the particle damping for a simple

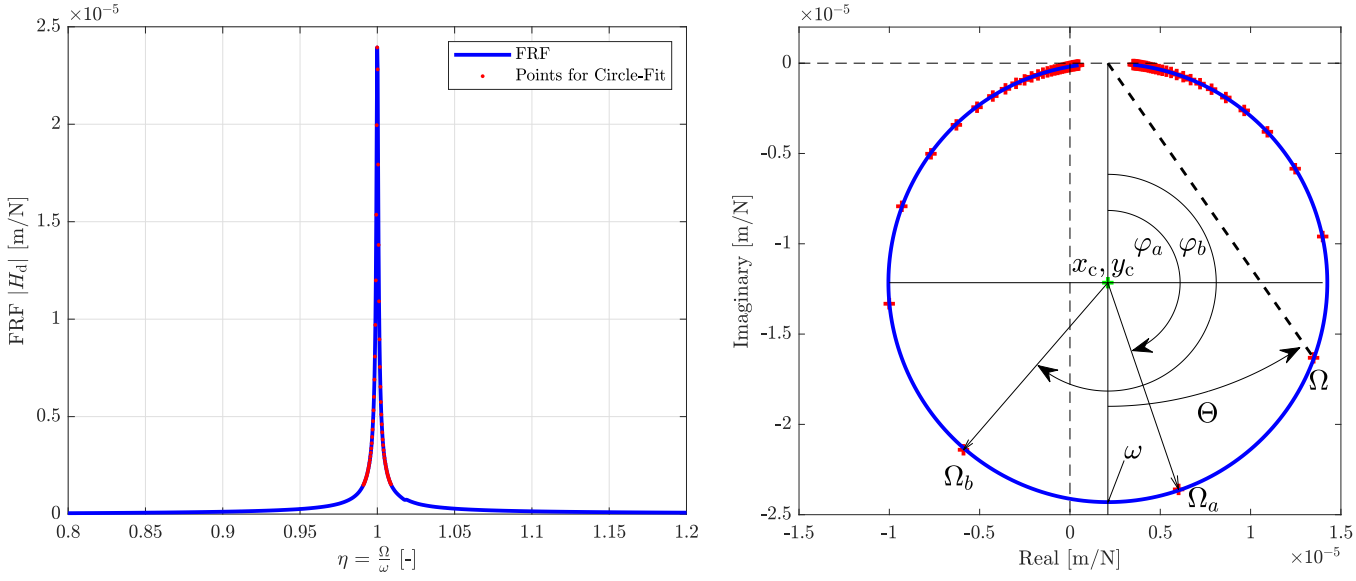

Fig. 4. Frequency response function (FRF) left, circle-fit right.

structure first. For this purpose, a DoE for the characterization of increased damping on beams is created in the following, the results of which are then to be transferred to other components.

3. Experimental methodology

This section describes the methodical procedure for the characterization of particle damping. Modal parameters can be used to analyze and compare dynamic systems with respect to geometric parameter changes for example. For this reason, in a first step a beam is used to evaluate the effect of particle damping for similar dynamic structures. The results may later be transferred to other parts, e.g. vibration-prone lightweight structures in aerospace applications. By means of a Design of Experiment (DoE), the influencing variables on particle damping, which have been presented in the state of the art, are to be quantified and processed in the form of performance curves. The curves are determined as a function of force and frequency.

The aim is to help the designer, who needs to keep amplitudes in certain range with known excitation force and natural frequencies, to estimate the damping of the potential particle damper via the given performance curves. Furthermore, it should be possible to implement the curves into an FEM model in order to model further applications in detail. Since potential applications of particle damping can be in a wide frequency range, a frequency range up to 18,000 Hz is investigated here. However, the focus is on the beam's first bending mode as this is assumed to be the most relevant one. In order to cover the wide frequency range beams with different dimensions and correspondingly different eigenfrequencies are printed. Transferability of the results to other applications is achieved by developing a multi-stage partial factorial experimental design in the DoE. First the machine and process parameters are described. Next, the relevant design parameters of the beam that have an influence on the component damping are identified and specified. After that, the beams are designed, considering the manufacturing restrictions. Subsequently, this section deals with the test setup and the test execution.

3.1. Machine and process parameter

An aluminum alloy AlSi10Mg is selected for the beams, as this material has a high performance index. The performance index indicates the ratio of component stiffness to mass, acc. to Ashby [54]. Especially in the aerospace industry it is essential to dampen vibrations and to have a high component stiffness with low mass. As manufacturing parameters the standard parameters of EOS for the LPBF system M280 are selected (Table 1). For the additive manufacturing process about 30% recycled powder and 70% new powder is used. After the building process, the beams are sawn from the building platform. The remaining support structures are broken off by mechanical force and no subsequent heat treatment of the beams is carried out. Furthermore, no mechanical finishing except sandblasting of the beams is carried out and the influence of surface roughness on the damping is not investigated. In order to analyze manufacturing deviations, computer tomograph (CT) scans are carried out on a selection of beams and the mass of all beams is measured. In addition, the packing density of the powder can be evaluated by means of a CT scan. The damping of the component is influenced by the design parameters, and the parameters during the test execution, such as the excitation force, which are described in the following.

Table 1
Machine, powder and process parameter for EOS M280 and AlSi10Mg.

Process parameter	**Unit**	**Stripes**	**Up-skin**	**Down-skin**
Hatching distance	mm	0.19	0.21	0.21
Scanning speed	mm/s	1300	1000	1150
Power	W	370	360	340
Thickness	mm	–	0.09	0.06
Overlap	mm	0.02	0.02	0.02
Exposer strategy	–	EOS_Direct part		
Machine parameter	**Unit**	**Value**		
Platform temp.	°C	160		
Layer thickness	mm	0.03		
Atmosphere	–	Argon		
Powder parameter	**Unit**	**Value**		
Particle size analysis Acc. to ISO 13320	Classification	d10	d50	d90
	µm	29	47	71
Reuse	%	30		
Powder production	–	Inert gas atomization		

3.2. Determination of the test parameters

In general, the design parameters can be divided into the following categories: topology, shape, dimensions, quantity, material, tolerances and surface [55]. A beam with a cavity is selected as basic topology. A rectangular cross-section is selected in order to ensure good reproducibility when carrying out the test. For example, in the case of a freely supported beam on foam base, round beams may start to roll after impulse and thus measurements are disturbed, and reproducibility is not guaranteed. Round beams furthermore are difficult to position if the anisotropy from the printing process is to be investigated. A rectangular cross-section is also selected for the shape of the cavity inside the beams, since self-supporting structures must be used for printing. If the beams are printed horizontally, they can be positioned on the edge and down skin angles of 45° are naturally maintained. In order to be able to produce the components in the manufacturing process also vertical, the ends of the cavity must be formed by a tapering dome. This ensures a self-supporting structure for upright and horizontal positioning (see Fig. 5). This way it is possible to investigate the influence of anisotropy on component damping for different samples.

Design parameters are the external and internal dimensions of the beam. In total, all beams examined in this work are manufactured in 4 batches. For the first two batches, the external dimensions are set at $20 \times 20 \times 200\ mm^3$ and the internal dimensions (cavity width, height and length) are varied.

Using the first batch the influence of anisotropy, cavity width, cavity height and cavity length is investigated and the results statistically verified. The effects of the anisotropy on the damping are determined by the analysis of standing and lying produced beams. In general, standing and lying printed beams with solid core are used as a reference for the evaluation of particle damping. Most beams with particle filling are printed vertically, as this allows more beams to fit into the available space. According to the literature, particle damping is at its maximum when the cavity volume is at its maximum, so large volumes are required. However, the restrictions of additive manufacturing, such as the minimum wall thickness, must be met. The statistical validation is done by printing three bars per parameter set.

In the second batch, smaller and larger cross-sections are printed horizontally. Then, batches 1 and 2 are measured and analyzed in the lab before batch 3 and 4 are created.

From the third batch onwards, only horizontally printed beams are used, for which no dome geometry is required. In the third batch, the outer dimensions of the beams are varied. Beams with an external cross-section of $10 \times 10\ mm^2$ and $5 \times 5\ mm^2$ at a length of 200 mm and beams with a cross-section of $20 \times 20\ mm^2$ at a length of 150 mm are examined. By varying the dimensions of the components, the natural frequency of the beams is consequently changed. The natural frequency plays a role for the transferability of the results, since the damping is frequency dependent. Furthermore, the influence of the cavity dimensions can be converted into a dimensionless quantity (ratio of inner

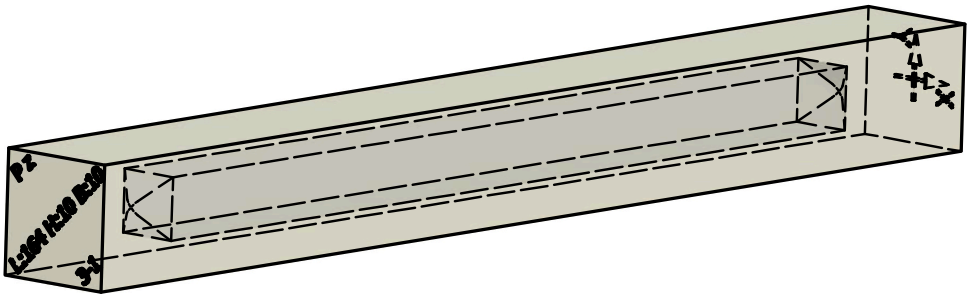

Fig. 5. Exemplary CAD model of a particle-filled beam with self-supporting structure for horizontal and vertical printing.

dimensions to outer dimensions) to simplify the transferability of the results to other structures.

In the fourth batch, the cavity width and cavity length are kept constant and the cavity height is varied on smaller scales in order to derive higher precision performance curves. The design parameter "number of cavities" is not varied (one cavity), because according to [8] a cavity subdivision leads to a decrease in component damping. In addition, a hollow beam without powder filling is manufactured in order to evaluate what kind of influence it has when the evaluation of the effect of the particle damping is carried out against either the fully-fused or the hollow beam.

3.3. Test plan

Table 2 shows the multi-stage partial factorial experimental design, which lists 26 parameter combinations of the test beams to be produced. A multi-stage partial factorial design means that only a selection of parameter combinations are examined in order to reduce the experimental effort and the number of samples to be produced to an acceptable level. The parameters build direction, length, width, height, cavity length, cavity width and cavity height are varied. In addition, there are two more parameters, force level and excitation direction, which are varied during the test procedure. The excitation force varies from 10 N to 180 N in steps of 10 N to 100 N and in steps of 40 N to 180 N. However, these values are deviated from in individual cases if, for example, the acceleration sensor reaches its saturation limit. In total, a 9-stage experimental design is available. This means that 9 parameters are varied. For the unique assignment of the beams, numbers were printed on the faces, as well as a coordinate system with which the positioning in the mounting space can be determined. The following notations were used for the axes:

- x-direction: Coater travel path
- y-direction: Perpendicular to coater travel path
- z-direction: Build direction.

Fig. 6 shows the first batch on the building platform, with marking of the building direction and the coater travel path. It can be seen that the three horizontally printed particle damped beams parameter (parameter 4) are positioned on the edge to maintain the required down-skin angles. Support structures are not shown in the figure, but were used in the construction job. At this point it should be noted once again that the cavities of beams 1–11 have been provided with a dome geometry at the ends so that the beams can be manufactured both horizontally and vertically. This allows the effect of the building direction on component damping to be analysed. The cavity length is calculated using the cavity volume. The cavity geometry of beams 12–26 is cuboid and without dome geometry, as the beams are only produced lying down. For the

Table 2
Test plan.

Parameter	Quantity	Batch	Build direction	Dome	Outer beam dimensions in mm			Cavity dimensions in mm			Cavity in %
					Length	Height	Width	Width	Height	Length	
1	3	1	y	Yes	200	20	20	Full material			
2	3	1	z	Yes	200	20	20	Full material			
3	3	1	z	Yes	200	20	20	10	10	164,68	20%
4	3	1	y	Yes	200	20	20	10	10	164,68	20%
5	3	1	z	Yes	200	20	20	10	5	164,3	10%
6	3	1	z	Yes	200	20	20	5	10	164,3	10%
7	3	1	z	Yes	200	20	20	10	10	162,06	10%
8	3	1	z	Yes	200	20	20	10	10	84,68	10%
9	3	1	z	Yes	200	20	20	10	10	44,68	5%
10	3	2	y	Yes	200	20	20	5	5	162,06	5%
11	3	2	y	Yes	200	20	20	15	15	78,5	20%
12	1	3	y	No	200	10	10	Full material			
13	1	3	y	No	200	10	10	5	5	160	20%
14	1	3	y	No	200	10	10	5	2,5	160	10%
15	1	3	y	No	200	5	5	Full material			
16	1	3	y	No	200	5	5	2,5	2,5	160	20%
17	1	3	y	No	200	5	5	2,5	1,25	160	10%
18	1	3	y	No	150	20	20	Full material			
19	1	3	y	No	150	20	20	10	10	120	20%
20	1	3	y	No	150	20	20	10	5	120	10%
21	1	3	y	No	200	20	20	10	10	164,68	20%
22	1	4	y	No	200	20	20	10	7,5	160	15%
23	1	4	y	No	200	20	20	10	5	160	10%
24	1	4	y	No	200	20	20	10	2,5	160	5%
25	1	4	y	No	200	20	20	10	10	160	20%
26	1	4	y	No	200	20	20	10	12,5	160	25%

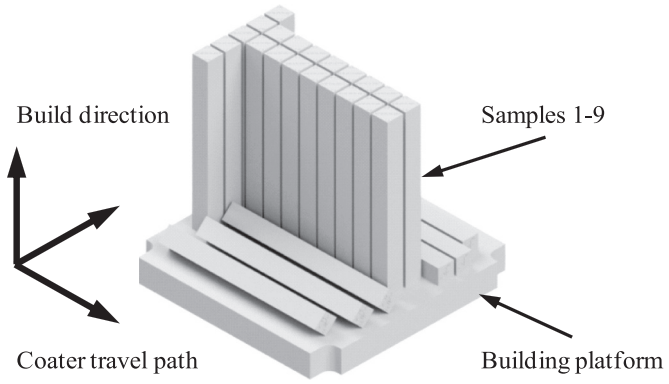

Fig. 6. Schematic representation of the first batch on the building platform.

transferability of the results, the variables cavity height to beam height, cavity width to beam width, cavity volume and natural frequency can be referred to.

3.4. Experimental setup

The beams are placed on a foam base and excited with an automated impulse hammer (see Fig. 7). Measuring equipment includes an impulse hammer 5800SL by Dytran, an acceleration sensor M353B17 by PCB Piezotronics and a data acquisition device VibRunner by m + p international. The software used for data acquisition and processing is the m+p Analyzer, which outputs the time data of the impulse hammer and the acceleration sensor and further the transfer function. Impulse excitation is preferred to sweep excitation with a shaker, as the beam need no clamping. Clamping the beam would cause parasitic friction, which would obscure the measured damping values. For example, Scott-Emuakpor et. al were unable to evaluate the first bending mode with a sweep due to the influence of beam clamping [2].

The impulse hammer is controlled in the lab by a motor. This means that it always hits the beam with high repetition accuracy, which a person cannot achieve. In addition, the force with which the beams are excited to vibrate can be adjusted via the automated impulse hammer. A further advantage is that double hits are prevented. Overall, the automated impulse hammer can significantly improve reproducibility. Two adjacent of the four long sides of each beam are examined to evaluate the effect of anisotropy. It is assumed that opposite sides behave identically. In contrast, different material properties are to be expected for the adjacent sides, especially for horizontally printed beams. The beam is supported on foam at the ends and excited in the center. The beams are each to be excited with 10 different forces and damping is calculated in the frequency domain using the Circle-Fit method.

4. Results

4.1. Determination of particle mass and packing density

As discussed in the state of the art, particle mass and packing density have a decisive influence on the effect of particle damping. To determine these quantities, the mass of all beams is measured with a scale and CT images are taken of selected beams. The particle mass of the parameter x can be calculated using the relationship in Eq. (3).

$$m_{\mathrm{P},x} = m_x - \frac{m_0}{V_0} \times V_x \tag{3}$$

Masses m_x and m_0 of the printed beams are measured with a scale and the beam volumes V_x and V_0 are determined from CAD. The index 0 indicates that it is the fully-fused (solid) beam with the same external dimensions as the beam under investigation. Packing density η can finally be determined by the ratio of densities ρ, see Eq. (4).

$$\eta_x = \frac{\rho_{\mathrm{P},x}}{\rho_0} \quad \text{with} \quad \rho_{\mathrm{P},x} = \frac{m_{\mathrm{P},x}}{V_0 - V_x} \tag{4}$$

Here $\rho_{\mathrm{P},x}$ represents the density of the particles in the cavity. Density of the particles is approximated to be equal to that of the fused material. In addition, manufacturing deviations lead to a difference between theoretical and real volume. Another influence may be the local porosity. Table 3 shows the results for beam mass, particle mass and

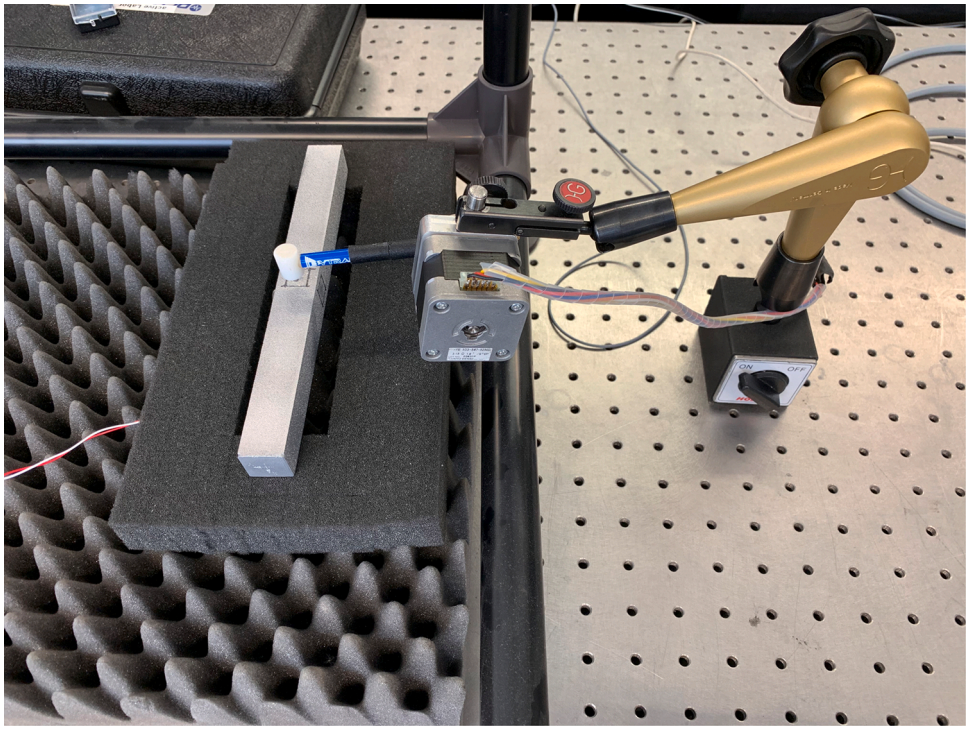

Fig. 7. Test setup for the characterization of particle damping.

Table 3
Beam mass m_B, particle mass m_P and packing density η of the beams.

Parameter	1	2	3	4	5	6	7	8	9	10	11	12	13
m_B [g]	212.20	207.38	191.55	192.92	198.78	200.15	191.71	199.33	205.23	206.83	193.02	53.75	48.45
m_P [g]	0	0	25.64	23.16	12.14	13.51	25.81	12.69	8.22	5.24	23.26	0	5.45
η [%]	1	1	61.83	54.56	58.53	65.12	62.23	61.18	79.27	49.42	54.80	1	50.70

Parameter	14	15	16	17	18	19	20	21	22	23	24	25	26
m_B [g]	50.85	13.95	13.05	12.5	159	144.2	151.2	171.05	197.45	197.6	206.6	193.05	188.50
m_P [g]	2.48	0	1.89	~ 0	0	17.00	8.1	–	17.08	6.62	5.01	23.29	29.35
η [%]	46.05	1	67.74	~ 1	1	53.46	50.94	–	53.66	31.20	47.22	54.88	55.33

packing density. For parameters 1–11 results of all 3 beam samples are averaged.

As can be seen from Table 3 the particle mass of the beams printed vertical is higher ($\overline{m_s} = 25.64$ g $> \overline{m_l} = 23.16$ g). The CT-images in Fig. 8 show that the beams are not completely filled with powder. The higher packing density of the upright printed beams is attributed to the coating in the construction process. Due to the weight of the powder itself, a higher packing density can be achieved in vertically printed components. The higher the powder is layered, the higher the weight force acting on the lower layers. This means that the lower layers of the beams printed upright are more compressed and more powder fits into the beams. It has also been found that a higher packing density can be realized in rectangular, non-square cross-sections when the shorter dimension of the cross-section points in the direction of the travel of the coater (parameter 5, 6).

The CT examination has shown that vertically printed beams have a significantly higher porosity from a height of 130 mm than horizontally printed beams. This is also confirmed by a higher mass of the horizontally printed beams (parameter 1 and 2). As the cavity volume increases, the packing density also increases. An exception are parameters 9 and 23, where the cavity volume is small and the calculated packing density is high. Possibly the high porosity in the beam leads to a wrong calculated packing density for parameter 9. Also, the scattering of the beam mass is high at this parameter, because the masses of the three printed beams of parameter 9 differ more than is usual for the other parameters. At parameter 23, the powder could have become stuck or be removed by the inert gas flow.

The results for parameter 17 suggest that there is no longer any unmelted powder in the cavity, as the unmelted powder has melted to the cavity wall. In order to evaluate what kind of influence it has when the evaluation of the effect of the particle damping is carried out against either the fully-fused or the hollow beam, a hollow beam is manufactured as parameter 21.

4.2. *Fully-fused beam*

For the evaluation of the particle damping effect, first the fully-fused (solid) beams are analyzed. The Circle Fit method is based on the values of the transfer function near the resonance point. Fig. 9 shows an example of the transfer functions of the fully-fused (solid) beams from the first batch with the dimensions $20 \times 20 \times 200$ mm^3.

The damping values D with well below 1% indicate a weakly damped system for all curves. First the horizontally printed beams (red and magenta curves) from Fig. 9 are analysed. It can be seen that the natural frequencies are shifted by about 30 Hz. From the 30 Hz higher natural frequency of the beams excited in the y-direction (magenta-colored curve) it can be concluded that the beams are stiffer in the y-direction than in the z-direction. This results in slightly anisotropic material properties. The curves of the vertically printed beams (cyan and blue) hardly differ in the direction of excitation and there are no significant anisotropic properties. It is noticeable that the natural frequency of the vertically printed beams is lower than that of the horizontally printed

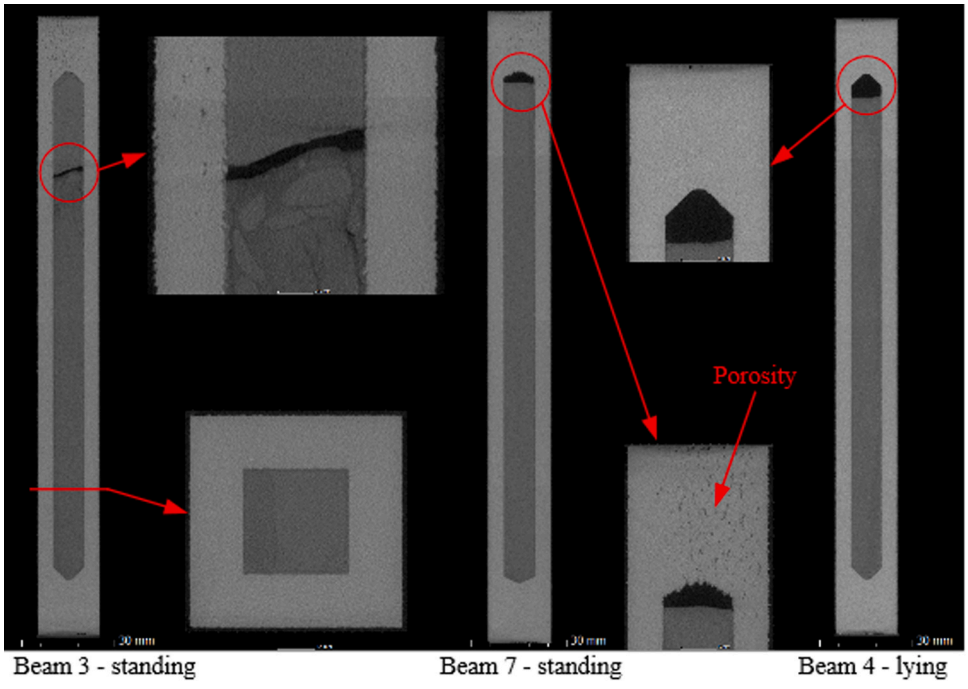

Fig. 8. CT scan of powder-filled beams.

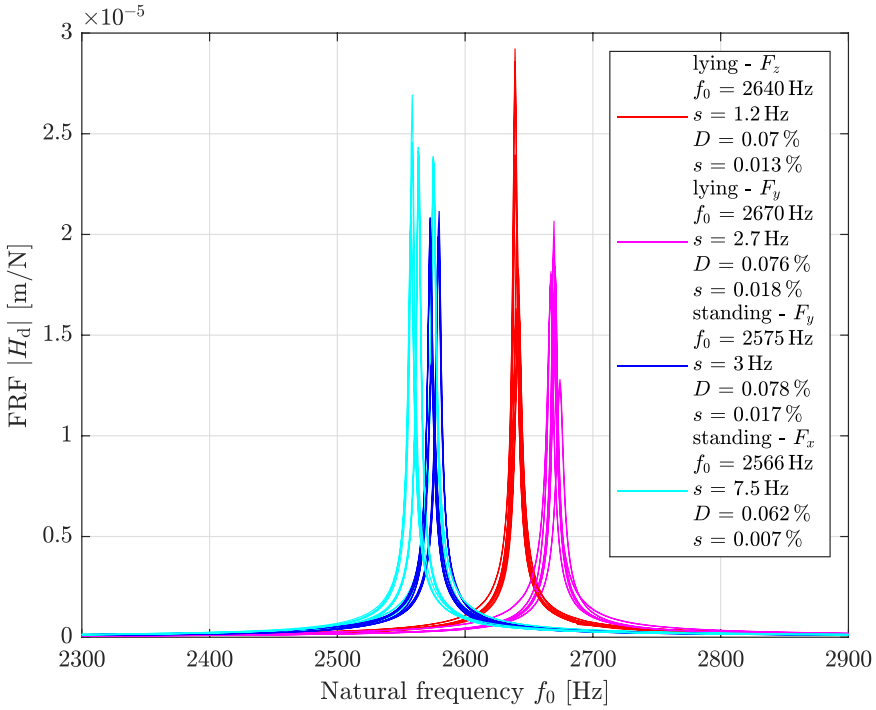

Fig. 9. Frequency response function of fully-fused beams, printed vertically and horizontally, parameter 1 and 2, dimensions: 20 × 20 × 200 mm^3. (For interpretation of the references to color in this figure, the reader is referred to the web version of this article.)

ones. Typically, the mechanical properties are better in *x*-, *y*-direction than in *z*-direction [56]. Thus the vertically printed beams should have had a higher natural frequency than the horizontally printed beams. According to Eq. (5) the natural frequency is proportional to Young's modulus *E*.

$$f_k = \frac{(\gamma_k \times L)^2}{2\pi} \times \sqrt{\frac{E \times I}{\rho \times A \times L^4}} \tag{5}$$

Eq. (5) is obtained from Euler–Bernoulli beam theory with γ_kx $\times L$ representing a factor depending on boundary conditions and on the considered mode. This can be looked up in the relevant literature. The other parameters are defined as: moment of resistance *I*, density ρ, cross-section *A* and length *L*.

A possible reason for the lower natural frequency of the vertically printed beams can be the higher porosity (cf. Fig. 8), which has a negative effect on the mechanical properties as well as the Young's modulus.

Fig. 10 shows the result of the Circle-Fit procedure exemplarily for a horizontally printed beam, which is vibrating in *z*-direction. Measurement data of the fully-fused (solid) beams are very well approximated by a circle shape.

In Fig. 11 damping of the fully-fused beams (Parameter 1, 12, 15, 18) over eigenfrequency is plotted. All beams are printed horizontally. The results shown represent an average of at least five measuring points taken at different force levels. The natural frequency is varied via the outer dimensions (cross-section or length) of the beams. Slight anisotropy can be seen for the different beams.

Measured values of the natural frequencies correspond well with the analytical Eq. (5) for the freely supported beam. The damping increases with lower natural frequency and decreases with increasing natural frequency. The approximation of all measuring points shows a hyperbola curve. This figure gives the designer a first overview how the damping of fully-fused beams made of AlSi10Mg behaves at different natural frequencies. According to this correlation, frequency-dependent values of the damping for AlSi10Mg may be stored for use in secondary software. The assumption of a constant damping value would lead to an error of 600% according to Fig. 11, if instead of the damping of at 500 Hz the damping of 5000 Hz would be used.

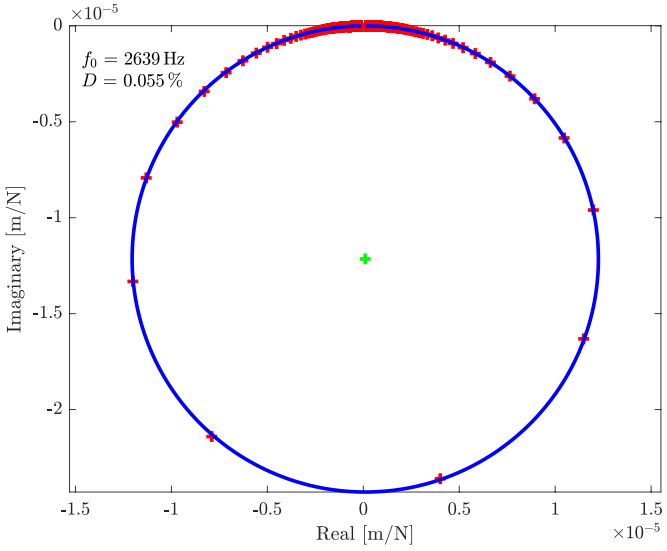

Fig. 10. Result of the circle fit method for a fully-fused beam, printed horizontally, excitation in *z*-direction, parameter 1.

In the tests, the beam width and beam length were varied. By analysing the equivalent 1 degree of freedom model it can be determined that the natural frequency increases with increasing beam width and decreases with increasing beam length. With the damping ratio it behaves the other way round, so that the damping decreases with increasing beam width and increases with increasing beam length. If now the damping ratio is plotted against the natural frequency, a hyperbola-shaped curve results. In this equivalent 1 degree of freedom mode, it is easy to understand that the damping measure is inversely proportional to the root of stiffness and mass.

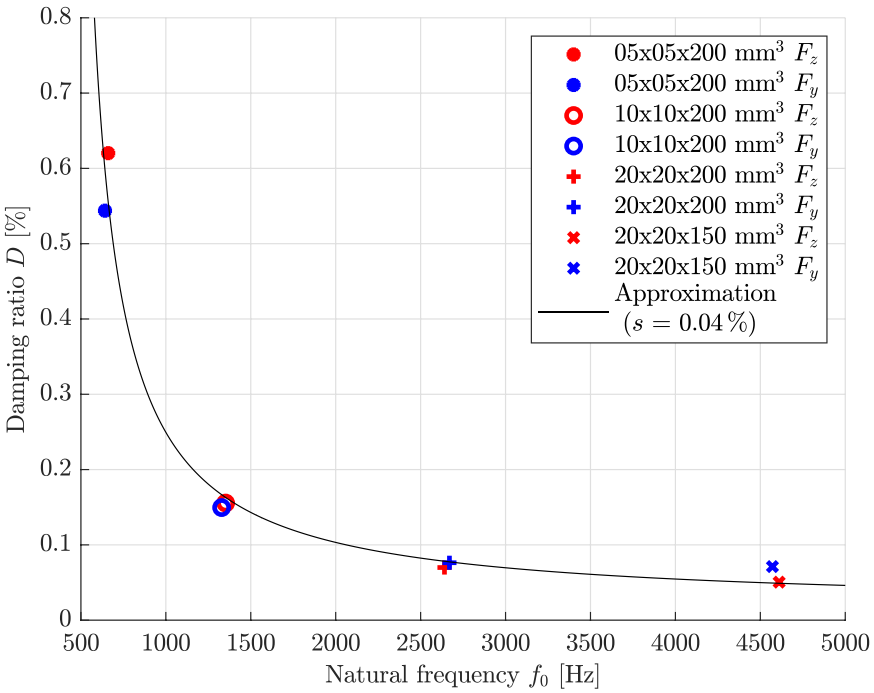

Fig. 11. Frequency dependent damping of fully-fused (solid) beams, parameter 2, 12, 15, 18.

4.3. Particle damped beams

Fig. 12 shows three FRFs of beams with dimensions 5 × 5 × 200 mm^3. The resonance peaks describe the 1., 3., 5., and 7. bending vibration mode, respectively. Modes 2, 4, and 6 are not visible in the transfer function, since the accelerometer position corresponds to a node of vibration of these modes. The fully-fused beam has the highest response values for each resonance. With particle damping, both 10% and 20% cavity portion give a considerable amplitude reduction in the observed frequency range of 600–18,000 Hz. Frequencies beyond that range could not be sufficiently be excited by the applied impulse hammer. Table 4 shows the values of amplitude reduction, for the damped beams compared to the fully-fused beam. It is noteworthy that a higher vibration reduction is achieved for the first and third bending mode by the larger cavity and for the fifth and seventh bending mode by

Table 4
Amplitude reduction of three 5 × 5 × 200 mm^3 beams, parameter 15–17.

Damped beam	1st mode	3rd mode	5th mode	7th mode
10% cavity	32%	48%	75%	76%
20% cavity	42%	75%	68%	58%

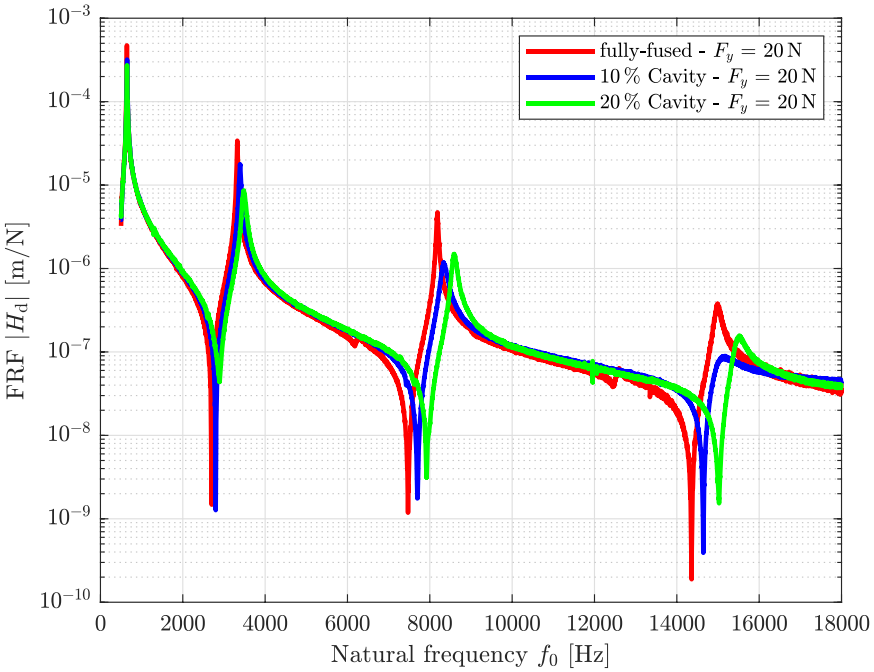

Fig. 12. Frequency response function of three 5 × 5 × 200 mm^3 beams, parameter 15–17.

the smaller cavity. For the first bending mode low additional damping could be achieved. However, the damping increases for the higher bending modes since beam deflections are higher at lower frequencies, but the powder will experience only little relative displacement. At higher frequencies, the beam deflections decrease and shift to the order of magnitude at which the powder moves. Thus, more energy is dissipated. It follows that a small cavity volume is more effective for higher bending modes than a large one.

The higher modes around 8 kHz and 15 kHz clearly reveal the nonlinear character of the parameter variation investigated. Cavity changes are associated with distinctive shift in resonance frequency and there is obviously an optimum cavity value for damping performance of each mode. Since the shift in natural frequency is negligible for the first bending mode the circle fit approximation is applicable here. In the following the focus is on the first bending mode of the beam.

Fig. 13 shows exemplarily a comparison of the transfer function of a fully-fused, a hollow and a particle-filled beam (parameters 1, 21, 25). All three beams are manufactured in horizontal position with dimensions of 20 × 20 × 200 mm^3. The hollow and particle-filled beams have a cavity of 10 × 10 × 160 mm^3 (20%). The powder-filled beam has the lowest amplitude and highest damping. Natural frequency of the particle-filled beam is in good agreement with the natural frequency of the hollow unfilled beam. Thus, the powder does not lead to any significant frequency shift and only non-linear damping occurs, which is why the Circle-Fit method can be applied. In the following, the particle damping is compared only to the fully-fused beams, so that fewer beams have to be printed. Furthermore, the values of the damping of the fully-fused and the hollow unfilled beam are of the same order of magnitude, so that the effect of particle damping can be quantified with sufficient accuracy. Fig. 14 shows the result of the Circle Fit method for the particle damped beam for which the FRF is shown in Fig. 13. Despite the nonlinear effects of particle damping in the resonance region, a good circle fit approximation is realized.

4.3.1. *Influence of the additive manufacturing process on particle damping*

In the following, the influence of the manufacturing process on the effect of particle damping is examined. On the one hand it is important to know how the vibration characteristics of standing and lying printed beams differ from each other. On the other hand, it is of interest how the vibration properties differ when the beams are excited to vibrate in *x*-, *y*- or *z*-direction. Fig. 15 makes clear that for both the standing and the lying printed beams (20 × 20 × 200 mm^3), directional excitation has no effect on the damping. The particle-filled beams have a cavity of 10 × 10 × 160 mm^3. It can be recognized that over the entire force level the damping is significantly higher than for the fully-fused beam (min. × 8). The damping of the fully-fused beam is approximately independent of the excitation force. For this test series, three beams each are manufactured in upright and horizontal position.

It is apparent that the damping of the particle-filled beams decreases with increasing force and asymptotically approaches a boundary value. As described in the literature, this can be attributed to the limited mobility of the particles at high forces. For example, at high forces the particles may move like a solid mass and have less friction and impact. The standing beams show higher damping for all forces investigated. This can be explained by a higher packing density of the beams (cf. Section 4.1).

The damping curve over the force is approximated by a hyperbola. Measurement results are more scattered at lower forces than at high forces. The deviations are attributed to several influences, such as variance in packing density. In addition, the CT images show that the powder in the beam does not necessarily have to rest at the bottom due to gravity. The reason for this can be poor flowability or increased friction between the particles. Consequently, the different distribution of the powder in the cavity can also have an influence on the dispersion of the damping. For example, repeated hammer impacts can cause the powder to be displaced in the beam, so that different damping values can be measured even at one force level. A force-independent influence on the scatter of the measured damping values can be the surface roughness, as this can influence the applied impulse.

4.3.2. *Variation of the cavity length*

Fig. 16 shows the influence of the cavity length (parameters 3, 8, 9)

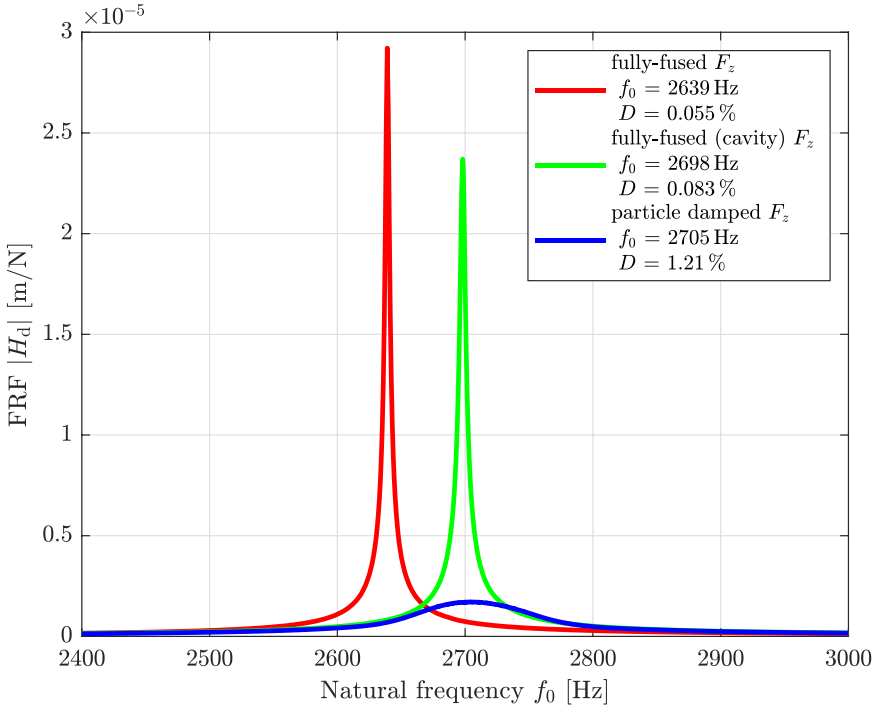

Fig. 13. FRF of a fully-fused and a particle damped beam (dimensions: 20 × 20 × 200 mm^3, cavity of the particle-filled beam: 10 × 10 × 160 mm^3, Force 100 N, parameter 2, 21, 25).

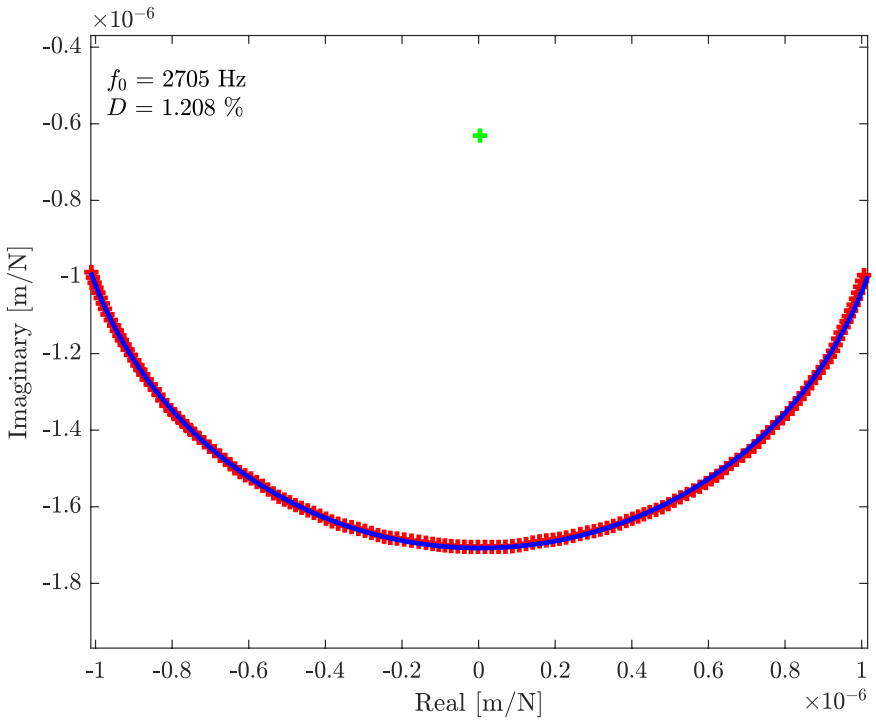

Fig. 14. Circle-fit of the particle damped beam, parameter 25.

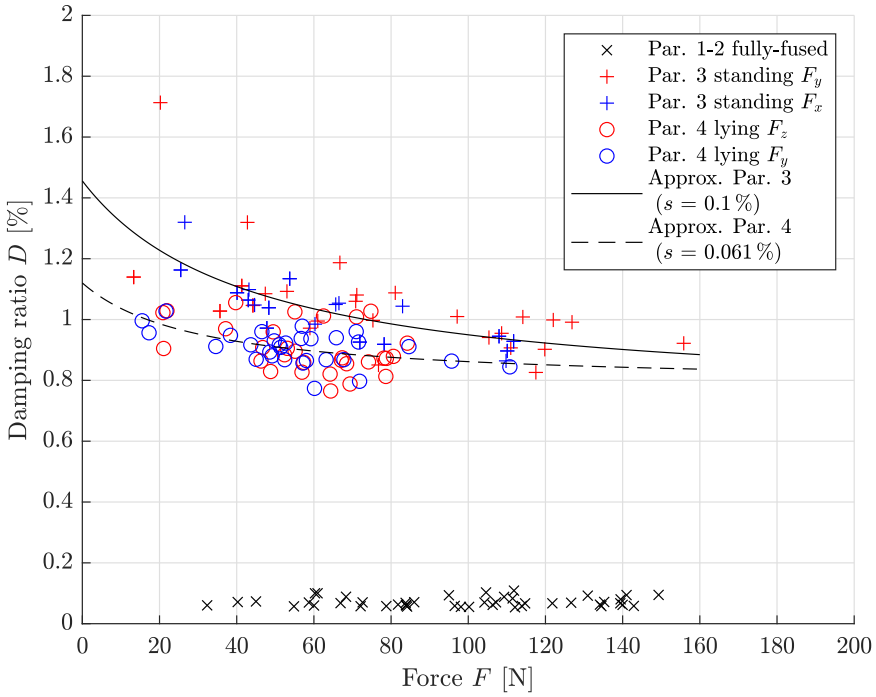

Fig. 15. Influence on particle damping – component orientation, Outer dimensions: 20 × 20 × 200 mm^3, parameter 1–4.

on the effect of particle damping. The vertically printed beams with the dimensions of 20 × 20 × 200 mm^3 have a cavity cross-section of 10 × 10 mm^2. The cavity is in the middle of all beams and three beams are produced per test series. The damping curves for the three particle-damped beams each approximately follow an exponential function. At 100 N the damping increased by about x6 for the smallest cavity length (5% powder filling), by about x9 for the middle one (10% powder filling) and by x10 for the large one (20% powder filling). It is notable that increasing the cavity length from 10% to 20% has no significant influence on the force-dependent damping, although the volume of the cavity is doubled. This is due to the fact that the particle-filled cavity is already present in the areas with large displacement of vibration. By further increasing the cavity length, particles are only added in regions with lower vibration deflection, which means that they do not make a significant contribution to vibration reduction. Another reason for the low damping of the small cavity is the high packing density of 79.27–62.23% or 61.18% (cf. Table 3).

Already at 50% of the normalized cavity length approx. 80% of the

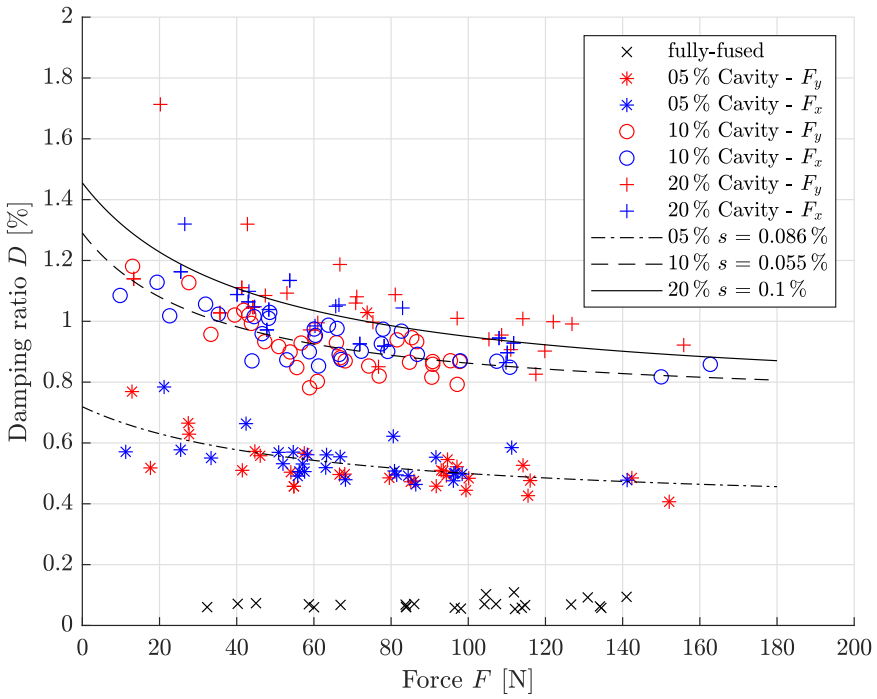

Fig. 16. Influence on particle damping – variation of cavity length, Outer dimensions: 20 × 20 × 200 mm^3, parameter 1, 3, 8, 9.

maximum possible damping is reached. After that, the damping increases only slightly. For the three series of measurements, the damping again decreases with increasing force in the form of a hyperbola.

The results so far indicate that the standard deviation of damping can be up to 0.1%. For all further test sequences starting with the third batch, only one beam per parameter is printed in order to keep the test effort in the lab low. Another reason is that all beams from the third batch onwards are printed horizontally, as the vertically printed beams have a high porosity (cf. Fig. 8). This means that fewer beams fit into one construction job. In order to keep the scattering in the further experiments low, the beams are preconditioned on a vibration plate to distribute the powder evenly in the cavity.

4.3.3. *Variation of the cavity height*

In the following the results of beams with external dimensions of 20 × 20 × 200 mm^3 and varied cross-section are described. The height of the cavity geometry (in z-direction) is varied at 2.5 mm intervals and the cavity width (y-direction) and the cavity positions are kept constant at 10 mm and 160 mm respectively. Results are shown in Fig. 17. Eigenfrequency of the fully-fused beams is around $f_0 = 2692.5$ Hz.

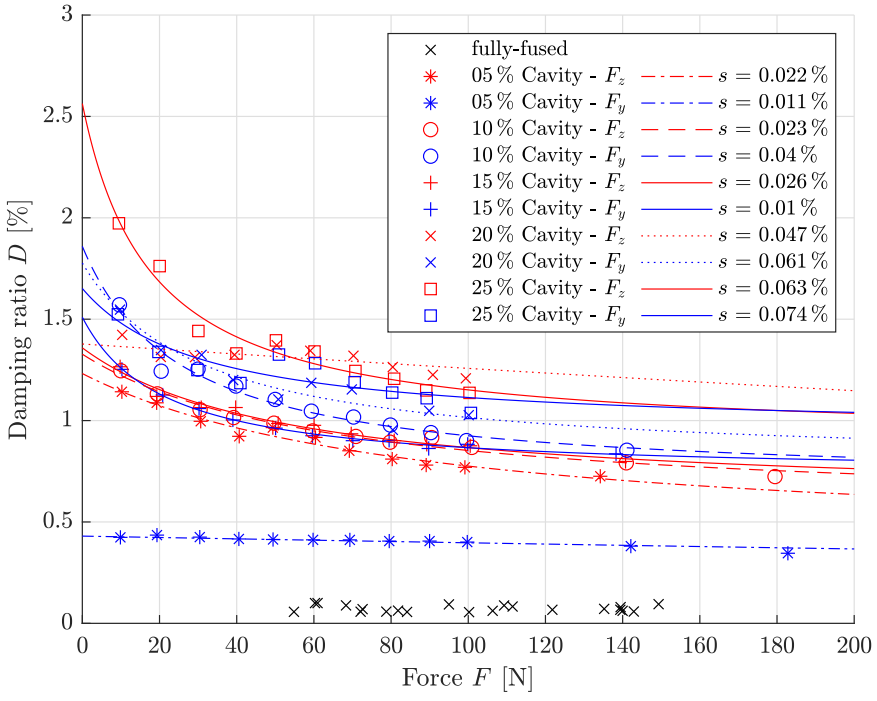

Fig. 17. Influence on particle damping – variation of cavity height, Outer dimensions: 20 × 20 × 200 mm^3, parameter 2, 22–26–17.

What is interesting is that only the smallest cavity volume (ratio of width to height: 4:1) exhibits pronounced directional properties. Apparently, the flowability of the particles in the y-direction is limited by the small cross-section in the direction of vibration, as the particles interlock with each other and with the wall. In the z-direction, on the other hand, the cross section in the direction of vibration is larger and the risk of some particles becoming entangled and blocking the path is lower. For beams with a cavity of 20% and 25% the damping increases by at least a factor of 15.

The damping increases non-linearly with continuous variation of the cavity height. Damping values with 10% cavity are higher than those with 15% cavity. This can be explained by the smaller packing density for the smaller cavity (31.20–53.66%). Although there are fewer particles in the smaller cavity, the lower packing density allows them to move easier and dissipate more energy.

In general, the dispersion of the measured values increases with increasing damping. The individual measurement curves are again approximated by a hyperbola function. Furthermore, before the test was carried out, the powder was evenly distributed inside the beam by vibration on a vibratory plate.

4.3.4. *Influence of the natural frequency*

In the following section the influence of the natural frequency on the effect of particle damping is examined. For this purpose, four beams with different external dimensions are manufactured in order to be able to evaluate the influence of the natural frequencies. One fully-fused beam and two particle-filled beams with a cavity of 10% and 20% are produced per outer beam dimension. The particle-filled beams differ in the cavity height. The larger cross-section is square, the smaller rectangular.

In the following the $5 \times 5 \times 200$ mm^3 beam is analyzed. This beam geometry represents the limits of production for additive manufactured particle dampers. On the one hand, the wall thickness of only 1.25 mm is very low, so there is an increased risk of powder leakage. On the other hand, the cavity is very small in relation to the particle size, so that the particles have limited space to move. Due to the limitations of the accelerometer, only forces up to 20 N can be investigated. It is obvious that the damping increases with increasing amplitude (cf. Fig. 18). The cross-sections in the beam are so small that the flow of the powder is reduced. For this reason, no large increases in damping can be seen. Damping possibly increases with increasing force, since the particles first must overcome the friction between them. In total, each force level was examined twice. In the case of the large cavity, a clear scattering of the measured values can be detected. The natural frequency of the fully-fused beams is $f_0 = 651.2$ Hz. Although a low damping could be realized for the first mode, the damping increases at higher modes (cf. Fig. 12).

In the following the results of the $10 \times 10 \times 200$ mm^3 beams are presented. Fig. 19 shows two additional resonances around the first eigenfrequency of the fully-fused as well as of the particle filled beam 13. This characteristic is exemplary for all measurements of parameters 12–14, and repositioning of the beams on the foam base also showed no change. It is possible that these side resonances are due to the thermal distortion of the beams, since the three beams are slightly curved. As the Circle Fit method is a single-degree method, it is not suitable for determining the damping in these cases. Nevertheless, a significant decrease in vibration amplitude can be noticed near the resonance of the fully-fused versus the particle-filled beams. For this reason, the amplitude decrease is calculated for each measured value by the ratio of the maximum resonance peak of the damped beam to the mean value of the fully-fused beam. Fig. 20 on the left shows that the amplitude can be reduced by up to 70–92%. The natural frequency of the fully-fused beams is $f_0 = 1342.3$ Hz. In order to convert the results to a damping value, the factor of the amplitude reduction is calculated with the damping of the fully-fused beams and thus an equivalent damping is calculated, see Fig. 20 right. Here the damping increases with increasing amplitude. For small cross-sections, the damping can be increased by $\times 5$ and for large cross-sections by $\times 10$. Thus, double the damping is realized for twice the volume of the cavity. Note that no direction-dependent damping values occur for the rectangular cavity cross section. The results are again approximated by a hyperbola.

The results for the $20 \times 20 \times 150$ mm^3 beams are described below. The damping decreases with increasing amplitude, see Fig. 21. The damping can be increased by at least $\times 3$ for the small cross-section and $\times 6$ for the large cross-section. Here again, no direction-dependent damping properties can be seen. The results are again approximated by a hyperbola. The natural frequency of the fully-fused beams is f_0

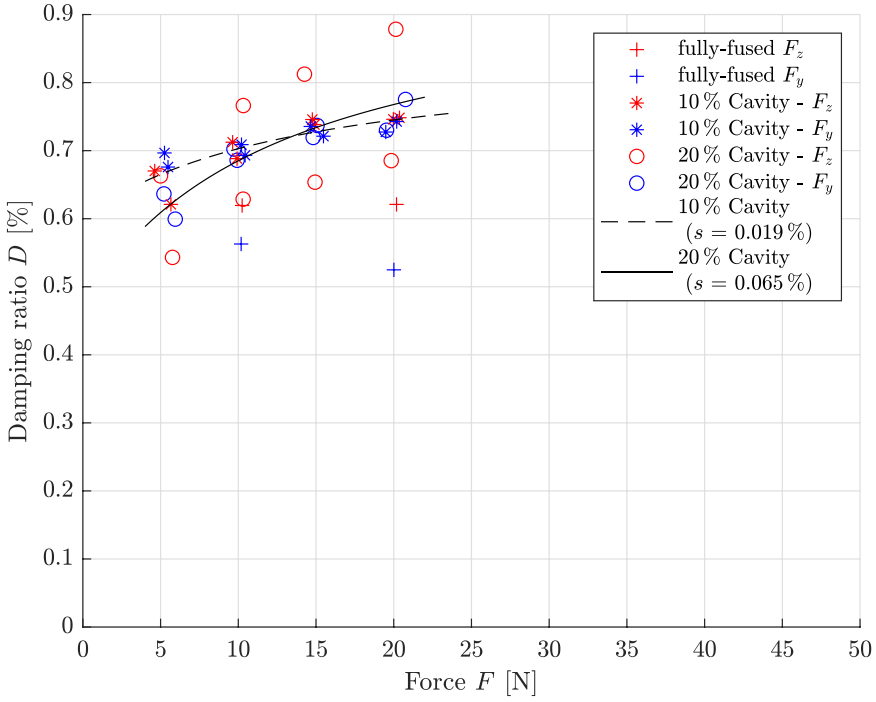

Fig. 18. Influence on particle damping – variation of the cavity cross section, Outer dimensions $5 \times 5 \times 200$ mm^3, parameter 15–17.

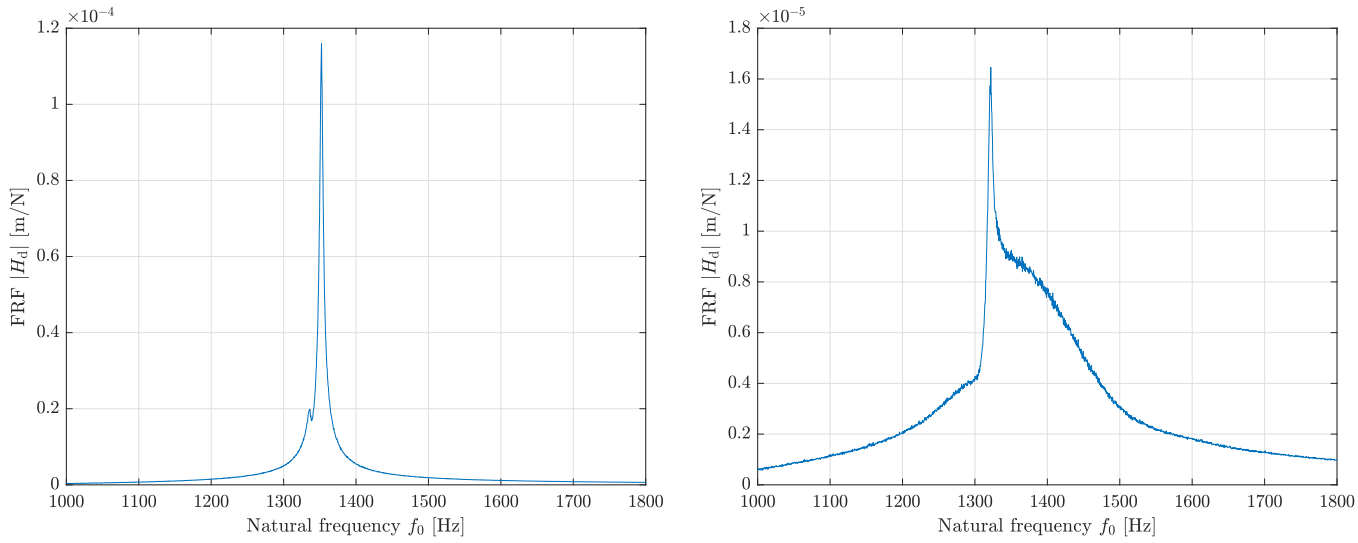

Fig. 19. Left: FRF of the fully-fused beam (Parameter 12, $F_z = 10$ N), right: FRF of the particle-filled beam (Parameter 13, $F_z = 10$ N), Outer dimensions 10 × 10 × 200 mm^3.

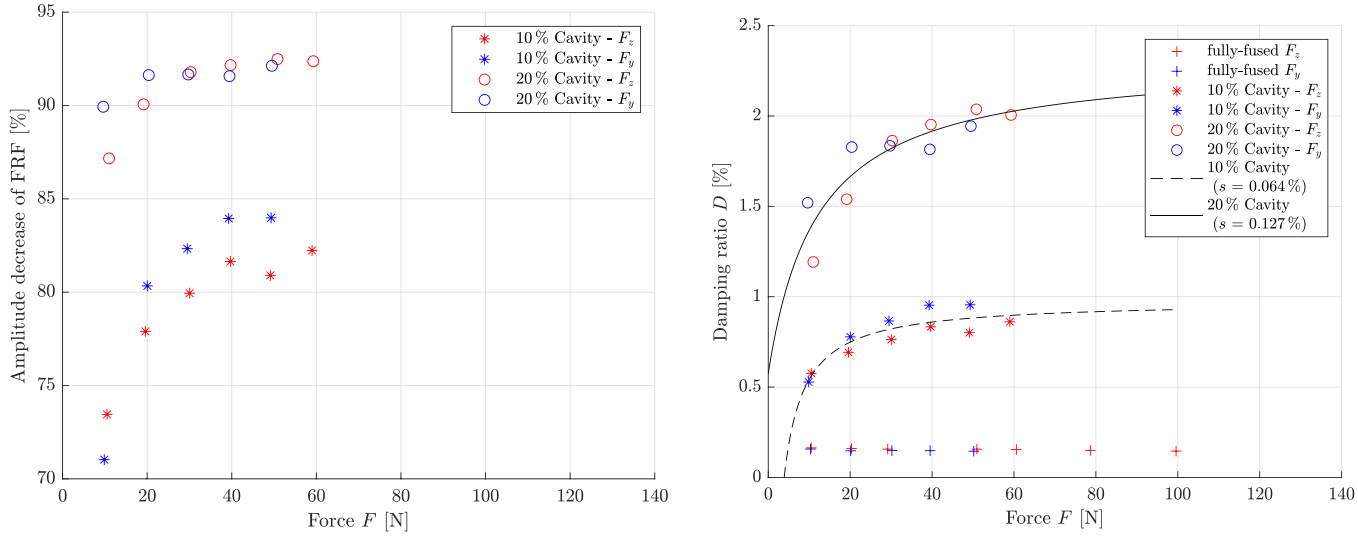

Fig. 20. Influence on particle damping – variation of the cavity cross section, outer dimensions 10 × 10 × 200 mm^3 parameter 12–14 Left: Amplitude decrease of the FRF, right: Equivalent damping.

= 4591.0 Hz.

4.4. Particle damping of higher bending modes

The following section describes the effect of particle damping at higher bending modes. Since the accelerometer is located in the middle of the beam, only odd bending modes are measured. For even bending modes, the accelerometer is located in the vibration node. Fig. 22 shows the damping of the third bending mode of the 10 × 10 × 200 mm^3 beams. Again, with increasing cavity height the damping increases significantly. It is evident that for the small cavity (10%) a direction-dependent damping occurs. For the first bending mode (see Fig. 20) this is not the case. Furthermore, the third bending mode shows no more side resonances, but a clear resonance peak. The natural frequency of the fully-fused beams is 6902 Hz. The damping values have decreased slightly compared to the first bending mode. Nevertheless, a quadrupling of the damping compared to the fully-fused beams is visible for the large cavity volume.

5. Discussion

Until now, laser melted particle dampers made of Inconel 718, AISI 316L stainless steel and tool steel 1.2709 have been investigated in the literature [7,8,14]. This paper shows that even with aluminum powder AlSi10Mg a damping of more than factor 20 can be realized. Furthermore, the damping of the first bending mode is shown in this paper. The assumption that the Circle Fit method – which is a single degree of freedom method and is used for linear systems – can also be used for highly non-linear systems of particle damping was confirmed. The first bending mode shows non-linear damping and no frequency shift and thus the Circle-Fit method has been justified. Overall, a robust test setup and method for test evaluation are defined.

The natural frequency can be used as a basis for transferring the results to other components designs. The simulation of particle-damped systems is still a particular challenge. The discrete element method (DEM) is very time consuming and computationally intensive. With the values of damping determined in this paper, a designer can estimate the damping if she/he knows what his critical frequencies and excitation

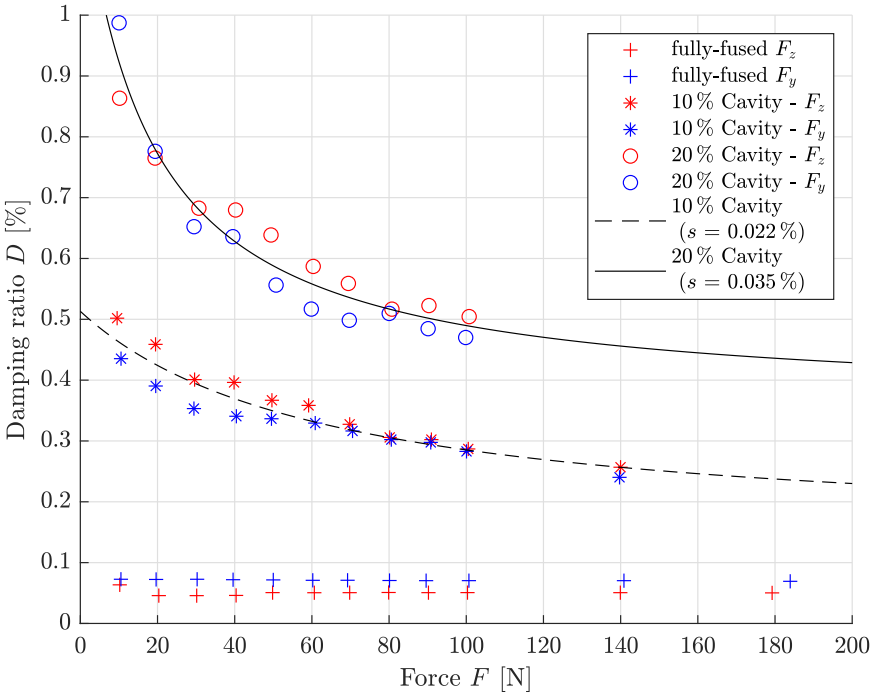

Fig. 21. Influence on particle damping – variation of the cavity cross section, Outer dimensions 20 × 20 × 150 mm^3, parameter 18–20.

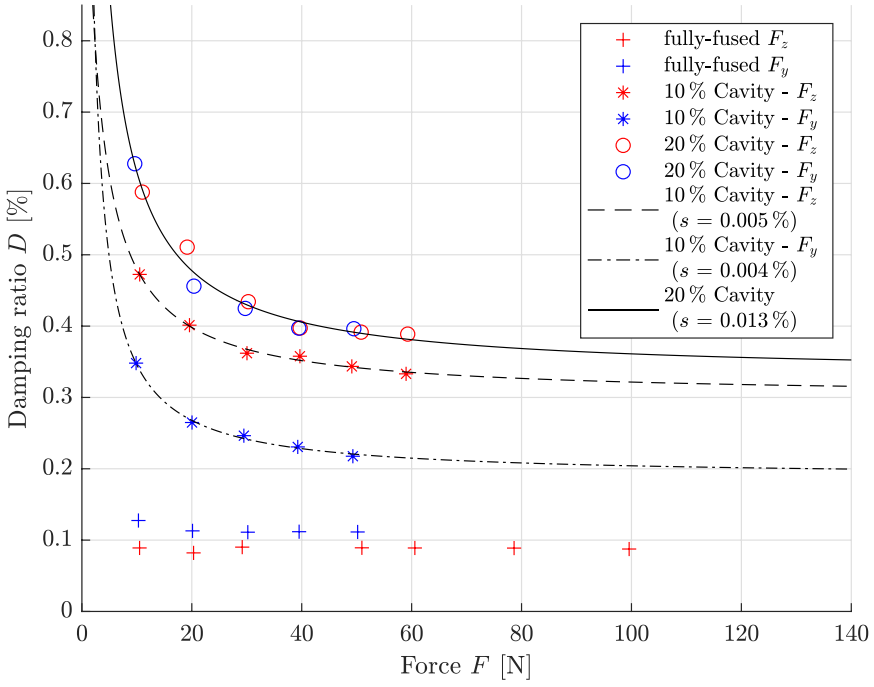

Fig. 22. Influence on particle damping – 3rd mode, variation of the cavity cross section, Outer dimensions 10 × 10 × 200 mm^3, parameter 12–14.

forces are. However, with the restriction of the vibration being similar to a bending mode. Based on this estimation, it can be evaluated whether it is worth the effort to use DEM or testing to get more detailed results. A comparison with the damping characteristics from this paper allows early estimations for or against the use of particle damping. Furthermore, inverse correlations with increasing natural frequency can be seen. Up to approx. 1500 Hz the damping increases with increasing force, whereas above approx. 1500 Hz the damping decreases with increasing force. At low frequencies there is low dynamics of particle movement in the system, so that the particles dissipate energy primarily through friction. The particles lying at the bottom are compressed by the weight of the particles lying at the top and cannot move easily. Furthermore, the static friction must be overcome. By increasing the excitation force, the static friction is overcome by a growing number of particles until finally all particles can move freely. In contrast, chaotic movements occur at high frequencies even with small forces due to the highly dynamic nature, which decreases when the force is increased. At higher forces, the particles behave like a single coherent mass, with the number of impacts decreasing. At high forces, in this case from 100 N, an asymptotic course of damping is observed, in which the energy

dissipation resulting from the effects of friction and impact is balanced.

In Fig. 23 a flow chart diagram is used as a framework to evaluate the effect of particle damping and transfer it to the desired component. A validation of the framework is still pending and must be tested in further work. The framework is designed to be as general as possible and the design curves built up in this work can be stored in a knowledge base. In further work, the aim should be to investigate further parameter studies on the load cases torsion, tensile and compression as well as a superposition of the load states and to store the results in the framework. Furthermore, this framework should be tested on real application examples such as a motorcycle triple clamp. A motorcycle triple clamp, for example, could be designed under the aspects of mass, stiffness and damping.

In the literature, the approach of integrating lattice structures into additively manufactured components in order to reduce vibrations is currently followed. Up to now, this method has mainly been used to reduce the component mass. The combination of lattice structures and particle damping can be a promising approach to reduce vibrations. In large cavities, down-skin angles of $\delta > 45°$ must be maintained in order to prevent the down-skin surfaces from sagging during the manufacturing process. For this purpose, lattice structures can be inserted into the powder-filled cavities. Alternatively, cavities for powder filling can be integrated into the lattice structures themselves. However, in this case the minimum cross-section of the individual lattice strut results from the minimum wall thickness and the minimum bore diameter in which the powder can still move freely. In this paper it is demonstrated that powder can be integrated in beams with $5 \times 5\ mm^2$. Using the manufacturing restrictions from Fig. 3, particle-filled cavities with a minimum cross-section of $2 \times 2\ mm^2$ could theoretically be produced. Compared to the initial model, this would increase damping and save mass.

Since particle-filled cavities can be integrated even in very narrow geometries, particle damping promises great potential in conjunction with topology optimization. By adapting target functions and manufacturing restrictions, cavities can be provided during topology optimization in areas particularly susceptible to vibration, in which powder can be stored. Especially for lightweight construction, components can thus be optimized in terms of mass, stiffness and damping.

The test results show that damping through particle-filled cavities within 600–18,000 Hz is effective. Lower and higher frequencies are not investigated in this work. However, the literature shows that conventional particle dampers are effective at only a few < 15 Hz [10,12,13]. For the first mode, a large cavity leads to higher damping. For higher modes, however, a smaller particle-filled cavity is more effective. Furthermore, at higher modes and thus higher frequencies, the random motion of particles in the cavity can increase, which can also lead to an increase in amplitude beyond the resonance. Accordingly, if several resonances are to be damped, a balance must be found between a large and a small cavity.

In contrast, one reason why laser melted particle dampers are not widely used, despite their distinctive properties, is that the powder is classified as hazardous to health and carcinogenic and must not escape in the event of cracks in the component shell. However, with the further development of the system technology for multi-material processing [46], it will be possible in the future to deposit non-harmful materials inside the component. Alternatively, the powder can be replaced after the construction process. Nevertheless, aerospace already represents an application area for particle damping with high potential.

6. Conclusion

In this paper the effect of particle damping on laser melted beams made of AlSi10Mg is experimentally characterized. It was found that the vibration amplitudes can be significantly reduced by particle damping from the first to the seventh bending mode and thus a broadband damping (here: 600–18,000 Hz) is realized. The damping could be

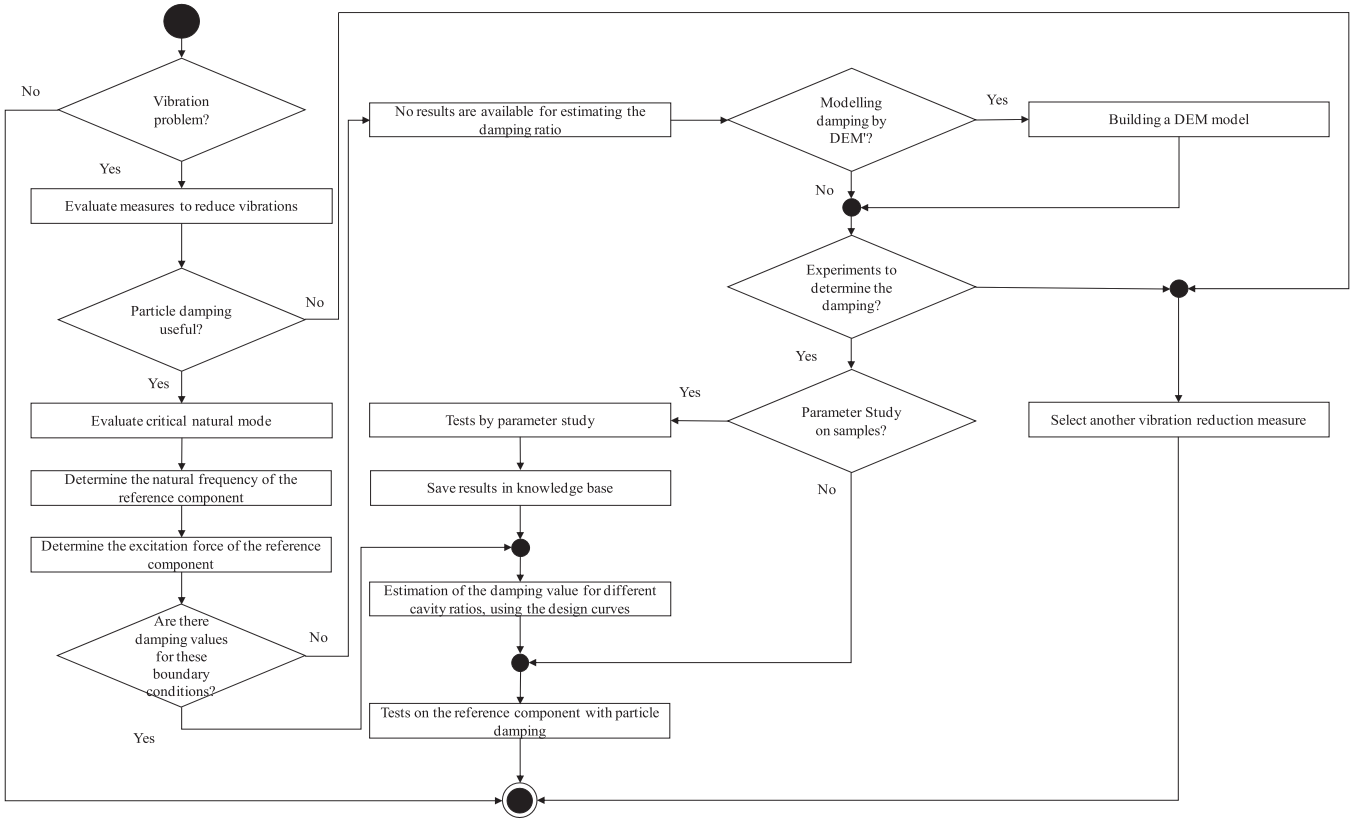

Fig. 23. Flow chart to evaluate the effect of particle damping and transfer it to the desired component.

increased for all particle-filled beams, in some even up to factor ×20. The cavity width and cavity height have a stronger influence on the damping than the cavity length. Vertically printed beams have a higher packing density and also higher damping than horizontally printed beams. One way to increase the damping of horizontally printed beams could be to change the particle size distribution towards smaller particles, as this would increase packing density. The damping curve is force-dependent and follows a hyperbola function, resulting in a nearly constant curve for forces above approx. 100 N. Furthermore, the damping for both the fully-fused and the particle-filled beams is frequency-dependent. The fully-fused beams have a hyperbola curve for damping over the natural frequency.

The higher bending modes in certain measurement series could not be evaluated because two side resonances were measured instead of one pronounced main resonance. In further work, it is necessary to optimize the positioning of the beams on the foam and to subject the beams to heat treatment. A heat treatment removes thermally induced stresses from the manufacturing process and reduces the beam deformation. In addition, the beam surfaces may be finished mechanically for increased reproducibility. Furthermore, the lifetime of particle-damped components will be evaluated in future work. Since the particle-filled cavities of additively manufactured particle dampers cannot be finished, the increased surface roughness can be regarded as a crack indicator for dynamically loaded structural components. However, it is possible that particle / wall interactions leading to erosion will rub off the roughness peaks of the cavity, thus reducing crack initiation. Also the long-term effect of additive manufactured particle dampers should be investigated to evaluate the degeneration of the component damping at high cycle numbers and excitation amplitudes. So far, only a few powder types have been investigated for the production of additive particle dampers. Highly inflammable powders such as titanium powder have the risk of reacting with oxygen, which can diffuse through the component shell. Here, the long-term chemical behavior of the powder in the cavities needs to be investigated. Correspondingly, further experiments are necessary with regard to the lifetime investigation. In addition, a surrogate model should be developed in further work. A better understanding of particle damping may open up new areas of application in space travel.

Declaration of Competing Interest

The authors declare that they have no known competing financial interests or personal relationships that could have appeared to influence the work reported in this paper.

References

[1] Z. Lu, Z. Wang, S.F. Masri, X. Lu, Particle impact dampers: past, present, and future, Struct. Control Health Monit. 25 (2017), e2058, https://doi.org/10.1002/stc.2058.

[2] O. Scott-Emuakpor, T. George, B. Runyon, C. Holycross, B. Langley, L. Sheridan, R. O'Hara, P. Johnson, J. Beck, Investigating damping performance of laser powder bed fused components with unique internal structures, in: Volume 7C: Structures and Dynamics, ASME, n.d., p. V07CT35A020. ⟨https://doi.org/10.1115/GT2018-75977⟩.

[3] O. Scott-Emuakpor, T. George, B. Runyon, B. Langley, L. Sheridan, C. Holycross, R. O'Hara, P. Johnson, Forced-response verification of the inherent damping in additive manufactured specimens, in: S. Kramer, J.L. Jordan, H. Jin, J. Carroll, A. M. Beese (Eds.), Mechanics of Additive and Advanced Manufacturing, Volume 8, Springer International Publishing, Cham, 2019, pp. 81–86, https://doi.org/10.1007/978-3-319-95083-9_15.

[4] O. Scott-Emuakpor, T. George, B. Runyon, J. Beck, L. Sheridan, C. Holycross, R. O'Hara, Sustainability study of inherent damping in additively manufactured nickel alloy, AIAA J. 57 (2019) 456–461, https://doi.org/10.2514/1.J057608.

[5] O.E. Scott-Emuakpor, T. George, J. Beck, B.D. Runyon, R. O'Hara, C. Holycross, L. Sheridan, Inherent damping sustainability study on additively manufactured nickel-based alloys for critical part, in: Proceedings of the AIAA Scitech Forum, American Institute of Aeronautics and Astronautics, Reston, Virginia, 23443, 2019. ⟨https://doi.org/10.2514/6.2019-0410⟩.

[6] O. Scott-Emuakpor, T. George, B. Runyon, C. Holycross, L. Sheridan, R. O'Hara, Assessing additive manufacturing repeatability of inherently damped nickel alloy components, J. Eng. Gas Turbines Power (2019), https://doi.org/10.1115/1.4044314.

[7] O.E. Scott-Emuakpor, J. Beck, B. Runyon, T. George, Multi-factor model for improving the design of damping in additively manufactured components, in: Proceedings of the AIAA Scitech Forum, American Institute of Aeronautics and Astronautics, Reston, Virginia, 13444, 2020. ⟨https://doi.org/10.2514/6.2020-1631⟩.

[8] T. Künneke, D. Zimmer, Funktionsintegration additiv gefertigter Dämpfungsstrukturen bei Biegeschwingungen, in: H.A. Richard, B. Schramm, T. Zipsner (Eds.), Additive Fertigung von Bauteilen Und Strukturen, Springer Fachmedien Wiesbaden, Wiesbaden, 2017, pp. 61–74, https://doi.org/10.1007/978-3-658-17780-5_4.

[9] T. Künneke, D. Zimmer, Schall mittels Pulver dämpfen, Konstruktionspraxis – Alles, Was DerKonstrukteur Braucht, 2019, 2019, pp. 24–26.

[10] A. Papalou, S.F. Masri, Performance of particle dampers under random excitation, J. Sound Vib. 118 (1996) 614–621, https://doi.org/10.1115/1.2888343.

[11] H.V. Panossian, Structural damping enhancement via non-obstructive particle damping technique, J. Vib. Acoust. 114 (1992) 101–105, https://doi.org/10.1115/1.2930221.

[12] R.D. Friend, V.K. Kinra, Particle impact damping, J. Sound Vib. 233 (2000) 93–118, https://doi.org/10.1006/jsvi.1999.2795.

[13] B.L. Fowler, E.M. Flint, S.E. Olson, Effectiveness and predictability of particle damping, in: T.T. Hyde (Ed.), Smart Structures and Materials 2000: Damping and Isolation, SPIE, 2000, pp. 356–367, https://doi.org/10.1117/12.384576.

[14] F.A.M. Vogel, S. Berger, E. Özkaya, D. Biermann, Vibration suppression in turning TiAl6V4 using additively manufactured tool holders with specially structured, particle filled hollow elements, Procedia Manuf. 40 (2019) 32–37, https://doi.org/10.1016/j.promfg.2020.02.007.

[15] D. Biermann, H. Meier, C. Haberland, H. Abrahams, M. Metzger, M. Steiner, Einsatz additiv gefertigter Werkzeughalter: Optimierungspotentiale beider Drehbearbeitung von Titan durch strahlgeschmolzene Werkzeugaufnahmen, WtWerkstattstechnik – Online: Forschung Und Entwicklung in Der Produktion, 2013, pp. 481–484.

[16] M. Schmitt, T. Kamps, C. Seidel, G. Reinhart, Affecting transmission NVH-behaviour by implementing a damping system using additive manufacturing, in: Proceedings of the Lasers in Manufacturing (LiM), 2017.

[17] N. Hopkinson, P.M. Dickens, R.J.M. Hague, Rapid Manufacturing: An Industrial Revolution for the Digital Age, John Wiley, Chichester, England, 2006, https://doi.org/10.1002/0470033991.

[18] V. Bhavar, P. Kattire, V. Patil, S. Khot, K. Gujar, R. Singh, A review on powder bed fusion technology of metal additive manufacturing, in: A.B. Badiru, V.V. Valencia, D. Liu (Eds.), Additive Manufacturing Handbook, CRC Press, 2017, pp. 251–253, https://doi.org/10.1201/9781315119106-15.

[19] T.M. Mower, M.J. Long, Mechanical behavior of additive manufactured, powder-bed laser-fused materials, Mater. Sci. Eng. A 651 (2016) 198–213, https://doi.org/10.1016/j.msea.2015.10.068.

[20] N. Contuzzi, S.L. Campanelli, F. Caiazzo, V. Alfieri, Design and fabrication of random metal foam structures for laser powder bed fusion, Materials 12 (2019), https://doi.org/10.3390/ma12081301 (Basel, Switzerland).

[21] C.Y. Yap, C.K. Chua, Z.L. Dong, Z.H. Liu, D.Q. Zhang, L.E. Loh, S.L. Sing, Review of selective laser melting: materials and applications, Appl. Phys. Rev. 2 (2015), 041101, https://doi.org/10.1063/1.4935926.

[22] R. Lachmayer, P.C. Gembarski, P. Gottwald, R.B. Lippert, The potential of product customization using technologies of additive manufacturing, in: J. Bellemare, S. Carrier, K. Nielsen, F.T. Piller (Eds.), Managing Complexity, Springer International Publishing, Cham, 2017, pp. 71–81, https://doi.org/10.1007/978-3-319-29058-4_6.

[23] V.J. Challis, X. Xu, L.C. Zhang, A.P. Roberts, J.F. Grotowski, T.B. Sercombe, High specific strength and stiffness structures produced using selective laser melting, Mater. Des. 63 (2014) 783–788, https://doi.org/10.1016/j.matdes.2014.05.064.

[24] H. Hanselka, Adaptronics as a key technology for intelligent lightweight structures, Adv. Eng. Mater. 3 (2001) 205–215, https://doi.org/10.1002/1527-2648(200104)3:4<205::AID-ADEM205>3.0.CO;2-H.

[25] P. Avdovic, A. Graichen, O. Rehme, M. Schäfer, Bauteil mit einem gefüllten Hohlraum, Verwendung dieses Bauteils und Verfahren zu dessen Herstellung, Registration number: 102010063725, Publication number: DE102010063725A1, Applicant: Siemens Aktiengesellschaft, Registered: 21.12.2010, Published: 21.06.2012.

[26] VDI-Gesellschaft Produkt- und Prozessgestaltung: VDI 2062 Blatt 1 – Schwingungsisolierung – Begriffe und Methoden: VDI-Handbuch Schwingungstechnik, Beuth, Deutschland/Berlin, 2011.

[27] S. Andresen, A. Bäger, C. Hamm, Eigenfrequency maximisation by using irregular lattice structures, J. Sound Vib. 465 (2020), 115027, https://doi.org/10.1016/j.jsv.2019.115027.

[28] L. Cheng, X. Liang, E. Belski, X. Wang, J.M. Sietins, S. Ludwick, Natural frequency optimization of variable-density additive manufactured lattice structure: theory and experimental validation, J. Manuf. Sci. Eng. 140 (2018), https://doi.org/10.1115/1.4040622.

[29] F. Rosa, S. Manzoni, R. Casati, Damping behavior of 316L lattice structures produced by selective laser melting, Mater. Des. 160 (2018) 1010–1018, https://doi.org/10.1016/j.matdes.2018.10.035.

[30] J.J. Hollkamp, R.W. Gordon, Experiments with particle damping, in: L.P. Davis (Ed.), Smart Structures and Materials 1998: Passive Damping and Isolation, SPIE, 1998, pp. 2–12, https://doi.org/10.1117/12.310675.

[31] W. Xiao, J. Li, S. Wang, X. Fang, Study on vibration suppression based on particle damping in centrifugal field of gear transmission, J. Sound Vib. 366 (2016) 62–80, https://doi.org/10.1016/j.jsv.2015.12.014.

[32] C. Zhang, T. Chen, X. Wang, K. Yu, Influence of cavity on the performance of particle damper under centrifugal loads, J. Vib. Control 22 (2016) 1704–1714, https://doi.org/10.1177/1077546314544351.
[33] S.S. Simonian, Particle beam damper, in: C.D. Johnson (Ed.), Smart Structures and Materials 1995: Passive Damping, SPIE, 1995, pp. 149–160, https://doi.org/10.1117/12.208884.
[34] K. Mao, M.Y. Wang, Z. Xu, T. Chen, Simulation and characterization of particle damping in transient vibrations, J. Sound Vib. 126 (2004) 202–211, https://doi.org/10.1115/1.1687401.
[35] S.E. Olson, An analytical particle damping model, J. Sound Vib. 264 (2003) 1155–1166, https://doi.org/10.1016/S0022-460X(02)01388-3.
[36] M. Saeki, Analytical study of multi-particle damping, J. Sound Vib. 281 (2005) 1133–1144, https://doi.org/10.1016/j.jsv.2004.02.034.
[37] B.L. Fowler, E.M. Flint, S.E. Olson, Design methodology for particle damping, in: D. J. Inman (Ed.), Smart Structures and Materials 2001: Damping and Isolation, SPIE, 2001, pp. 186–197, https://doi.org/10.1117/12.432703.
[38] H. Pourtavakoli, E.J.R. Parteli, T. Pöschel, Granular dampers: does particle shape matter? N. J. Phys. 18 (2016), 073049 https://doi.org/10.1088/1367-2630/18/7/073049.
[39] M. Masmoudi, S. Job, M.S. Abbes, I. Tawfiq, M. Haddar, Experimental and numerical investigations of dissipation mechanisms in particle dampers, Granul. Matter 18 (2016) 71, https://doi.org/10.1007/s10035-016-0667-4.
[40] S.C. Dragomir, M. Sinnott, E.S. Semercigil, Ö.F. Turan, Energy dissipation characteristics of particle sloshing in a rotating cylinder, J. Sound Vib. 331 (2012) 963–973, https://doi.org/10.1016/j.jsv.2011.09.010.
[41] P. Veeramuthuvel, K.K. Sairajan, K. Shankar, Vibration suppression of printed circuit boards using an external particle damper, J. Sound Vib. 366 (2016) 98–116, https://doi.org/10.1016/j.jsv.2015.12.034.
[42] B. Sathishkumar, K.M. Mohanasundaram, M.S. Kumar, Impact of particle damping parameters on surface roughness of bored surface, Arab. J. Sci. Eng. 39 (2014) 7327–7334, https://doi.org/10.1007/s13369-014-1209-1.
[43] T. Ehlers, R. Lachmayer, Einsatz additiv gefertigter Partikeldämpfer – eine Übersicht, in: R. Lachmayer, K. Rettschlag, S. Kaierle (Eds.), Konstruktion Für Die Additive Fertigung 2019, Springer Berlin Heidelberg, Berlin, Heidelberg, 2020, pp. 123–142, https://doi.org/10.1007/978-3-662-61149-4_9.
[44] Z. Xiang, M. Yin, Z. Deng, X. Mei, G. Yin, Simulation of forming process of powder bed for additive manufacturing, J. Manuf. Sci. Eng. 138 (2016), https://doi.org/10.1115/1.4032970.
[45] C. Anstaett, C. Seidel, Multi-material processing: next step in laser-based powder bed fusion, Laser Tech. J. 13 (2016) 28–31, https://doi.org/10.1002/latj.201600027.
[46] A. Bedoret, K. Eckes, M. Hick, Device and method for manipulating particles, Registration number: 2017071039, Publication number: WO002018059833A1, Applicant: Aerosint SA, Registered: 21.08.2017, Published: 05.04.2018.
[47] R.B. Lippert. Restriktionsgerechtes Gestalten gewichtsoptimierter Strukturbauteile für das Selektive Laserstrahlschmelzen (Dissertation), 2018, https://doi.org/10.15488/3489.
[48] R.B. Lippert, R. Lachmayer, A design method for SLM-parts using internal structures in an extended design space, in: M. Meboldt, C. Klahn (Eds.), Industrializing Additive Manufacturing – Proceedings of the Additive Manufacturing in Products and Applications – AMPA2017, Springer International Publishing, Cham, 2018, pp. 14–23. ⟨https://doi.org/10.1007/978-3-319-66866-6_2⟩.
[49] J. Günther, S. Leuders, P. Koppa, T. Tröster, S. Henkel, H. Biermann, T. Niendorf, On the effect of internal channels and surface roughness on the high-cycle fatigue performance of Ti-6Al-4V processed by SLM, Mater. Des. 143 (2018) 1–11, https://doi.org/10.1016/j.matdes.2018.01.042.
[50] J. Kranz, D. Herzog, C. Emmelmann, Design guidelines for laser additive manufacturing of lightweight structures in TiAl6V4, J. Laser Appl. 27 (2015), S14001, https://doi.org/10.2351/1.4885235.
[51] T. Ehlers, R. Lachmayer, S. Vajna, T. Halle, Producibility, in: S. Vajna (Ed.), Integrated Design Engineering, Springer International Publishing, Cham, 2020, pp. 287–323, https://doi.org/10.1007/978-3-030-19357-7_9.
[52] D.J. Ewins. Modal Testing: Theory, Practice and Application, 2nd ed., Research Studies Press, Baldock, 2000. ⟨http://www.loc.gov/catdir/enhancements/fy0745/97043590-d.html⟩.
[53] N.M. Mendes Maia, Extraction of Valid Modal Properties from Measured Data in Structural Vibration, 1988.
[54] M.F. Ashby, D. Cebon, Materials selection in mechanical design, J. Phys. IV 03 (1993) C7–1-C7-9, https://doi.org/10.1051/jp4:1993701. France.
[55] B. Sauthoff, P.C. Gembarski, R. Lachmayer, Maturity-model-based design of structural components, in: Proceedings of the DESIGN 2016 14th International Design Conference, 2016, pp. 503–512.
[56] M. Tang, P.C. Pistorius, Anisotropic mechanical behavior of AlSi10Mg parts produced by selective laser melting, JOM 69 (2017) 516–522, https://doi.org/10.1007/s11837-016-2230-5.